Spectroscopy of the $T = \frac{3}{2}$ $A = 47$ and $A = 45$ mirror nuclei via one- and two-nucleon knockout reactions

S. Uthayakumaar,[1] M. A. Bentley [ORCID],[1,*] E. C. Simpson,[2] T. Haylett,[1] R. Yajzey,[1,3] S. M. Lenzi,[4] W. Satuła,[5] D. Bazin,[6,7]
J. Belarge,[6] P. C. Bender,[6] P. J. Davies,[1] B. Elman,[6,7] A. Gade,[6,7] H. Iwasaki,[6,7] D. Kahl,[8,9] N. Kobayashi,[6] B. Longfellow,[6,7]
S. J. Lonsdale,[8] E. Lunderberg,[6,7] L. Morris,[1] D. R. Napoli,[10] T. G. Parry,[11] X. Pereira-Lopez,[1,12] F. Recchia,[4,6]
J. A. Tostevin,[11] R. Wadsworth,[1] and D. Weisshaar[6]

[1]*School of Physics, Engineering and Technology, University of York, Heslington, York YO10 5DD, United Kingdom*
[2]*Department of Nuclear Physics and Accelerator Applications, Research School of Physics,*
Australian National University, ACT 2601, Australia
[3]*Department of Physics, Faculty of Science, Jazan University, Jazan 45142, Saudi Arabia*
[4]*Dipartimento di Fisica e Astronomia dell'Università and INFN, Sezione di Padova, I-35131 Padova, Italy*
[5]*Institute of Theoretical Physics, Faculty of Physics, University of Warsaw, ul. Pasteura 5, PL-02-093 Warsaw, Poland*
[6]*National Superconducting Cyclotron Laboratory, Michigan State University, East Lansing, Michigan 48824, USA*
[7]*Department of Physics and Astronomy, Michigan State University, East Lansing, Michigan 48824, USA*
[8]*School of Physics and Astronomy, University of Edinburgh, Edinburgh EH9 3FD, United Kingdom*
[9]*Extreme Light Infrastructure–Nuclear Physics, Horia Hulubei National Institute for R&D in Physics and Nuclear Engineering (IFIN-HH),*
077125, Bucharest-Măgurele, Romania
[10]*INFN, Laboratori Nazionali di Legnaro, I-35020 Legnaro, Italy*
[11]*Department of Physics, Faculty of Engineering and Physical Sciences, University of Surrey, Guildford, Surrey GU2 7XH, United Kingdom*
[12]*Center for Exotic Nuclear Studies, Institute for Basic Science (IBS), Daejeon 34126, Republic of Korea*

Level schemes of the proton-rich nuclei, ^{47}Mn ($Z = 25$, $N = 22$) and ^{45}Cr ($Z = 24$, $N = 21$), have been established for the first time. The technique of mirrored one- and two-nucleon knockout reactions was applied to the secondary beams of ^{48}V/^{48}Mn and ^{47}V/^{47}Cr to populate states in ^{47}Ti/^{47}Mn and ^{45}Sc/^{45}Cr, respectively. Mirror energy differences (MED) have been studied between the mirrored $T = \frac{3}{2}$ states for both mirror pairs and interpreted using both a shell-model approach and a density-functional-theory approach using the no-core configuration-interaction method. MED in this mass region provide a stringent test of the model prescriptions since both *fp*- and *sd*-shell orbitals are active and, in ^{45}Cr, spherical and well-deformed structures coexist near the ground state. The inclusive and exclusive one-nucleon removal cross sections have been determined for the populated states in ^{47}Ti/^{47}Mn and compared with results from reaction-model calculations.

I. INTRODUCTION

Under the assumption that the nuclear force is charge symmetric and charge independent, the energy spectra for mirror nuclei would be expected to be identical apart from the contributions from electromagnetic effects. This symmetry, resulting from the approximately charge-invariant nature of the nuclear force, leads naturally to the fundamental concept of isospin symmetry [1] in which the proton and neutron are treated as two states of the same particle, the nucleon. In order to distinguish between these two types of fermions,

the neutrons and protons are assigned the isospin quantum number $t = \frac{1}{2}$. Each nucleon species is assigned a projection (t_z) in which the proton is assigned a value of $t_z = -\frac{1}{2}$ and the neutron having $t_z = \frac{1}{2}$. Hence, the total isospin projection of the nucleus, denoted by T_z, is given by:

$$T_z = \frac{(N - Z)}{2}. \tag{1}$$

States in nuclei of the same mass number and the same isospin quantum number, T, are known as isobaric analog states (IAS), with mirror nuclei being the most straightforward example. In mirror nuclei, where the number of protons and neutrons are interchanged, it is the charge symmetry of the nucleon-nucleon interaction that results in the isospin symmetry. These IAS will be degenerate in the absence of isospin-breaking interactions, such as the Coulomb interaction. In reality, the energy spectra of mirror nuclei demonstrate shifts in the excitation energies. It can be inferred that the

---

*Corresponding author: michael.bentley@york.ac.uk

excitation energy differences of the IAS result from isovector effects that break the effective charge symmetry ($V_{nn} \neq V_{pp}$). The Coulomb interaction between protons will dominate these contributions, but charge-symmetry breaking (CSB) of the nucleon-nucleon interaction itself will also contribute. It is the combination of these isospin nonconserving (INC) effects that lift the degeneracy of the analog states.

Differences in the excitation energies between mirror nuclei, known as mirror energy differences (MED), are defined as:

$$\text{MED}_J = E^*_{J,T,-T_z} - E^*_{J,T,T_z}, \tag{2}$$

where E^*_{J,T,T_z} is the excitation energy of a particular state that has a total angular momentum (spin) J, overall isospin T, and isospin projection T_z. MED studies provide excitation energy differences as a function of spin which correspond to isovector energy differences (e.g., Ref. [2]).

There have been extensive studies that explore MED between mirror pairs in the fp shell, e.g., Refs. [3–9]. Developments to shell-model calculations have allowed for a reliable theoretical analysis of MED based on multipole and monopole contributions of electromagnetic origin, based on the work of Zuker *et al.* [10]. That work, and other recent studies (e.g., Refs. [2,11]) have demonstrated that, in the shell-model framework, these Coulomb and magnetic effects are insufficient to account for experimentally observed MED in the $f_{\frac{7}{2}}$ region. This has resulted in the need for the inclusion of an additional effective isovector contribution, which has a strong J dependence (see Ref. [2]).

The motivation to study the MED in the ^{47}Ti/^{47}Mn and ^{45}Sc/^{45}Cr ($T_z = \pm\frac{3}{2}$) mirror pairs is as follows. First, the ^{47}Ti/^{47}Mn mirror nuclei exhibit a large difference in their neutron/proton separation energies and it is of interest to understand the extent to which weak binding in the proton-rich member of the mirror pair affects the underlying symmetry of the analog states. Indeed, apart from the first excited state, *all* states in ^{47}Mn are expected to be above the proton separation energy of 0.38 MeV. Second, these MED provide a stringent test of the shell-model approach in this lower-$f_{7/2}$ region, due to the complexity of the valence-space needed for realistic calculations. For shell-model calculations of the $A = 47$ and 45 ($T_z = \pm\frac{3}{2}$) mirror pairs, if the model space is restricted to fp-shell orbitals only, then one of the two nucleon species in each nucleus has only two ($A = 47$) or one ($A = 45$) active particles, and it is likely that the exclusion of N-particle N-hole excitations from the sd shell hampers the effectiveness of the shell-model approach. Moreover, in the ^{45}Sc/^{45}Cr mirror pair, a coexistence of low-lying (deformed) positive- and (spherical) negative-parity bands near the ground state is exhibited [12], the former most likely built on a single $d_{3/2}$ particle-hole excitation. Finally, since this presents a challenging case to the shell-model approach, it provides an opportunity to test the newly developed density-functional-theory approach [13] based on the no-core configuration-interaction (NCCI) model [14]. This has recently been applied and tested in the deformed $A = 80$ region [15].

The study of the $A = 47$ mirror pair applies the technique of mirrored one-nucleon removal reactions, first employed by Milne *et al.* [5], and subsequently applied to the $A = 70$ $T = 1$ mirrors [16], the $A = 55$ $T = \frac{1}{2}$ mirrors [17] and most recently to the $A = 48$ $T = 2$ mirrors [8]. The work presented here is from data gathered in the same experiment as the $A = 48$ $T = 2$ case [8]. The mirrored knockout approach used in the current work allows "mirrored" cross-section measurements to be made. The very different degrees of binding between the two mirror nuclei is of interest here, since published systematics [18–20] suggest that experimentally determined knockout strength (for reactions on light targets), in comparison to theory, shows a strong dependence on the asymmetry of the neutron and proton separation energies. Yajzey *et al.* [8] have recently performed a detailed analysis, in this context, of analog inclusive cross sections, and (tentative) exclusive cross sections, with large asymmetries in the cross sections discussed in terms of differences in nuclear binding. Analysis of the knockout cross sections to the $A = 47$ mirror nuclei is presented in the current work. For the $A = 45$ mirror nuclei, establishing the level scheme of ^{45}Cr has been achieved using a two-nucleon removal reaction, the technique first applied to the $A = 51$ ($T_z = \pm\frac{3}{2}$) mirror nuclei [6].

Using these approaches, the first level schemes of the excited states of the proton-rich, $T_z = -\frac{3}{2}$ nuclei, ^{47}Mn and ^{45}Cr have been tentatively established. The analog nature of the mirrored knockout reactions, as well as the direct nature of the reactions utilized, has been exploited to give confidence to the level schemes of the proton-rich members of the pair, based on the comparisons with the well established level schemes of the $T_z = +\frac{3}{2}$ mirror partners, ^{47}Ti [21] and ^{45}Sc [12], respectively. Using these level schemes, the MED have been established for these mirror pairs, presenting a stringent test of the state-of-the-art nuclear structure models, including (i) a shell-model approach in the fp valence space, (ii) including the possibility of a single $d_{3/2}$ excitation in one of the nucleon species, and (iii) a density-functional-theory (DFT) approach based on the NCCI model [13,14].

II. EXPERIMENTAL PROCEDURE

The experiment was performed at the National Superconducting Cyclotron Laboratory (NSCL) at Michigan State University (MSU), using the A1900 separator [22] and the S800 spectrograph [23]. A primary ^{58}Ni beam was accelerated to an energy of ≈ 160 MeV/u by the coupled K500 and K1200 cyclotrons and was impinged on a 802 mg/cm^2 ^{9}Be production target. The resulting radioactive isotopes produced from the fragmentation reaction were magnetically separated and identified using the A1900 fragment separator [22]. For the single A1900 setting that was used for knockout to the proton-rich systems studied, the cocktail of secondary radioactive beams, at the focal plane of the A1900, consisted of 0.5% ^{49}Fe, 5% ^{48}Mn, and 30% ^{47}Cr as well as other intense, lower-Z $N = 23$ isotones. The secondary beams were identified by time of flight (ToF) between the scintillator at the Extended Focal Plane of the A1900 and the Object scintillator (OBJ) in the S800 analysis line. These secondary beams impinged on a 188 mg/cm^2 ^{9}Be target, at the reaction-target position of the S800 spectrograph [23].

TABLE I. Details of the four reactions used in this work. Three different A1900/S800 settings were used.

Fragment of interest	Secondary beam	Reaction	Energy (MeV/u)	Rate[b] (pps)
^{47}Mn	^{48}Mn[a]	$-1n$	~ 84	$\sim 4 \times 10^3$
^{47}Ti	^{48}V	$-1p$	~ 89	$\sim 1 \times 10^5$
^{45}Cr	^{47}Cr[a]	$-2n$	~ 81	$\sim 3 \times 10^4$
^{45}Sc	^{47}V	$-2p$	~ 85	$\sim 1 \times 10^5$

[a]Same A1900/S800 setting.
[b]Estimated secondary beam rate.

At this location, states in the ^{47}Mn and ^{45}Cr ($T_z = -\frac{3}{2}$) nuclei were populated through one- and two-neutron knockout reactions from the $T_z = -1$ ^{48}Mn and $T_z = -\frac{1}{2}$ ^{47}Cr secondary beams, respectively. Both beams were present in the same A1900 fragment cocktail. The residual nuclei from the knockout reactions were identified in the S800 spectrograph using energy loss-ToF measurements. Energy loss was recorded using an ionization chamber and ToF was measured between the OBJ scintillator and a scintillator located at the end of the S800 spectrograph. Both measurements were corrected for the angle and position of the fragments at the S800 focal plane using the tracking information of the ions from the S800 position-sensitive detectors [23].

The ^{47}Ti and ^{45}Sc ($T_z = +\frac{3}{2}$) mirror partners of the two nuclei, which are well known, were populated using the "analog" (mirrored) reactions. ^{47}Ti (mirror of ^{47}Mn) was populated via one-proton knockout from $T_z = +1$ ^{48}V (the mirror of ^{48}Mn). Similarly, ^{45}Sc was produced via two-proton removal from $T_z = +\frac{1}{2}$ ^{47}V (the mirror of ^{47}Cr). However, it should be noted that, unlike 2n removal from ^{47}Cr, 2p removal from ^{47}V cannot be considered to be purely a direct two-proton knockout reaction, since the two-step reaction—proton knockout followed by proton evaporation—is also energetically feasible and is likely to be the dominant reaction pathway. Thus, the two reactions leading to the $A = 45$ mirrors cannot be considered as equivalent. The ^{48}V and ^{47}V secondary beams were produced in two separate, dedicated settings of the A1900 separator. A summary of the reactions used to study the four nuclei of interest is provided in Table I.

The prompt in-flight γ rays produced due to deexcitation at the secondary ^{9}Be target were detected by the Gamma-Ray Tracking In-beam Nuclear Array (GRETINA) [24,25], surrounding the secondary target. The configuration of GRETINA consisted of nine detector modules (36 crystals) in two rings, five of which were centered around 90° and four that were centered at 58° with respect to the beam axis [24]. This range covered laboratory angles from 37° to 115°. Each detector module consists of four 36-fold segmented HPGe crystals. Pulse-shape analysis was used to identify the position and energy of all γ-ray interactions and that with the highest-energy deposited was assumed to be the first interaction point [24]. To enhance photo-peak efficiency and to optimize the resulting γ-γ coincidences, a "cluster add-back" procedure was applied where the energies deposited within the neighboring crystals were added if they were detected within a cone
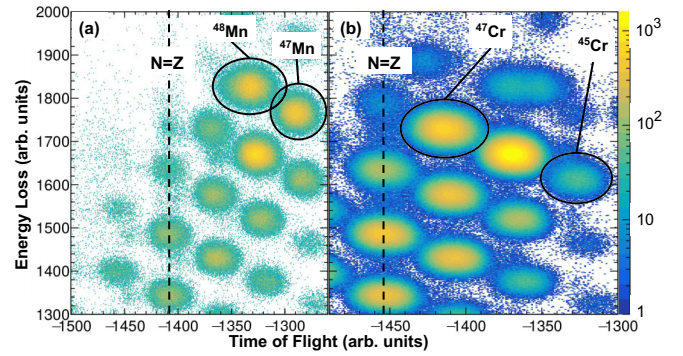

FIG. 1. The outgoing Particle Identification plot for the projectile-like reaction residues emerging from the target produced by gating on (a) the ^{48}Mn secondary beam and (b) the ^{47}Cr secondary beam. The plot shows the outgoing residues produced at the secondary target. Nuclei were identified by measuring the energy loss in the ionization chamber located at the focal plane of the S800 spectrometer as function of time of flight; see text for details.

of a certain angle. The optimum angle used was observed, in the current work, to depend on the multiplicity of the γ rays detected, and hence the cluster add-back angle of 15° was used for the energy spectra of ^{47}Ti and an angle of 20° was applied to ^{47}Mn, ^{45}Sc, and ^{45}Cr. This add-back procedure was not applied when obtaining the quoted efficiency-corrected γ-ray intensities, which are used in the analysis of exclusive cross sections.

III. RESULTS AND DISCUSSION

A. Level schemes of ^{47}Mn and ^{47}Ti

To produce γ-ray spectra, the incoming secondary beam and outgoing residue were selected as described above. Figure 1 shows the outgoing residue identification plot determined from the S800 detectors for the ^{48}Mn secondary beam (left) and the ^{47}Cr secondary beam (right). The measured velocity vector, reconstructed from the trajectories of the projectile-like residues in the S800 spectrograph, was combined with the first-interaction point of the γ ray within the GRETINA detector to enable a precise Doppler correction to be made on an event-by-event basis. The Doppler-corrected γ-ray spectra for ^{47}Ti and ^{47}Mn, produced by the one-nucleon knockout reactions from ^{48}V and ^{48}Mn, respectively, are presented in Figs. 2(a) and 2(d). All ^{47}Ti transitions observed in Fig. 2(a) are known [21] while all transitions observed in Fig. 2(d) are new. The optimum average recoil velocity, $\beta = \frac{v}{c}$, utilized to perform Doppler corrections, was determined by varying β until the angular dependence of the γ-ray energy with the polar angle in GRETINA (θ) is eliminated. The effective velocity also depends on the cumulative lifetime of the state from which the γ ray is emitted. The transit time through the secondary 1-mm-thick ^{9}Be target is of the order of 10 ps, and hence fast decays of the order of a few ps will decay within the target with a velocity that is higher, on average, than that for transitions that decay downstream of the target. The majority of the states observed in ^{47}Ti are known to have lifetimes that are <3 ps, apart from the 159-keV
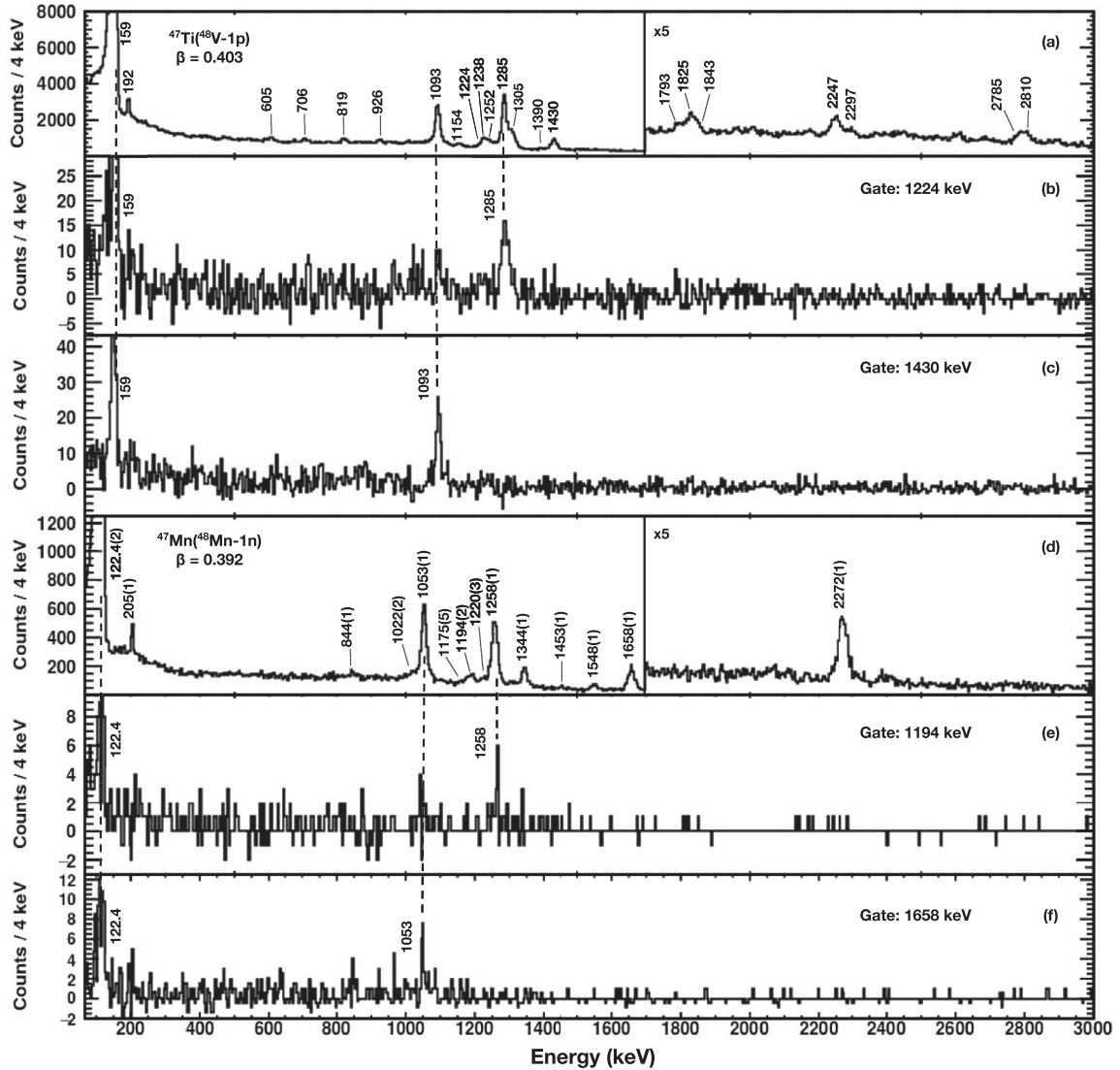
FIG. 2. The Doppler-corrected spectra produced by using cluster add-back (see text) for (a) ^{47}Ti and (d) ^{47}Mn from a one-proton (neutron) removal reaction from ^{48}V (^{48}Mn), respectively. The β value obtained for both (a) and (d) was optimized for "fast" transitions: 1093 keV in ^{47}Ti where the lifetime of the decaying $\frac{11}{2}^{-}_{1}$ state is <1 ps and its analog transition of 1053 keV in ^{47}Mn. Panels (b) and (c) show γ-γ coincidence spectra by gating on the 1224- and 1430-keV transitions in ^{47}Ti. The respective γ-γ coincidence analysis for their analog transitions in ^{47}Mn are shown in (e) and (f) by gating on the 1194- and 1658-keV transitions.

state, for which the current evaluation [21] lists a lifetime of $\tau = 303(9)$ ps. The values of $\beta = 0.403(5)$ and $0.392(5)$ were found for ^{47}Ti and ^{47}Mn, respectively, to optimize the peaks seen in Figs. 2(a) and 2(d). The typical in-beam γ-ray energy resolution for this experiment was of the order of 1.3% at an energy of ≈ 1.3 MeV.

The long lifetime of the 159-keV state results in a low-energy tail on this peak—and also for the analog transition around 122 keV in ^{47}Mn—see below. This tailing occurs since the decay takes place at an unknown position several cm downstream of the target, resulting in a spread of effective detector angles for the Doppler shift. Since Doppler correction assumes decays at the target position, this results in a downward shift in the peak energy and a long tail.

To identify excited states in ^{47}Mn, produced by a one-neutron knockout from ^{48}Mn, a comprehensive understanding

of which states are populated in the known ^{47}Ti nucleus, via the mirrored reaction, is an ideal starting point. The left side of Fig. 3 shows the partial level scheme of ^{47}Ti observed in this work. The ordering of this scheme has been confirmed through a γ-γ coincidence analysis and is in full agreement with earlier work [26]. Example coincidence spectra, gated on the 1224- and 1430-keV transitions, are shown in Figs. 2(b) and 2(c), respectively. All the γ-ray energies measured in ^{47}Ti in this work are consistent with published values in the current evaluation [21].

Figure 3 (left) shows that the majority of γ-ray transitions observed come from negative-parity states. Specifically, the populated negative-parity states are the yrast states with $J^{\pi} = \frac{5}{2}^{-}, \frac{7}{2}^{-}, \frac{9}{2}^{-}, \frac{11}{2}^{-}, \frac{13}{2}^{-}$, and $\frac{15}{2}^{-}$ and the yrare states of $J^{\pi} = \frac{7}{2}^{-}, \frac{9}{2}^{-}, \frac{11}{2}^{-}, \frac{13}{2}^{-}$, and $\frac{15}{2}^{-}$. These states can all be
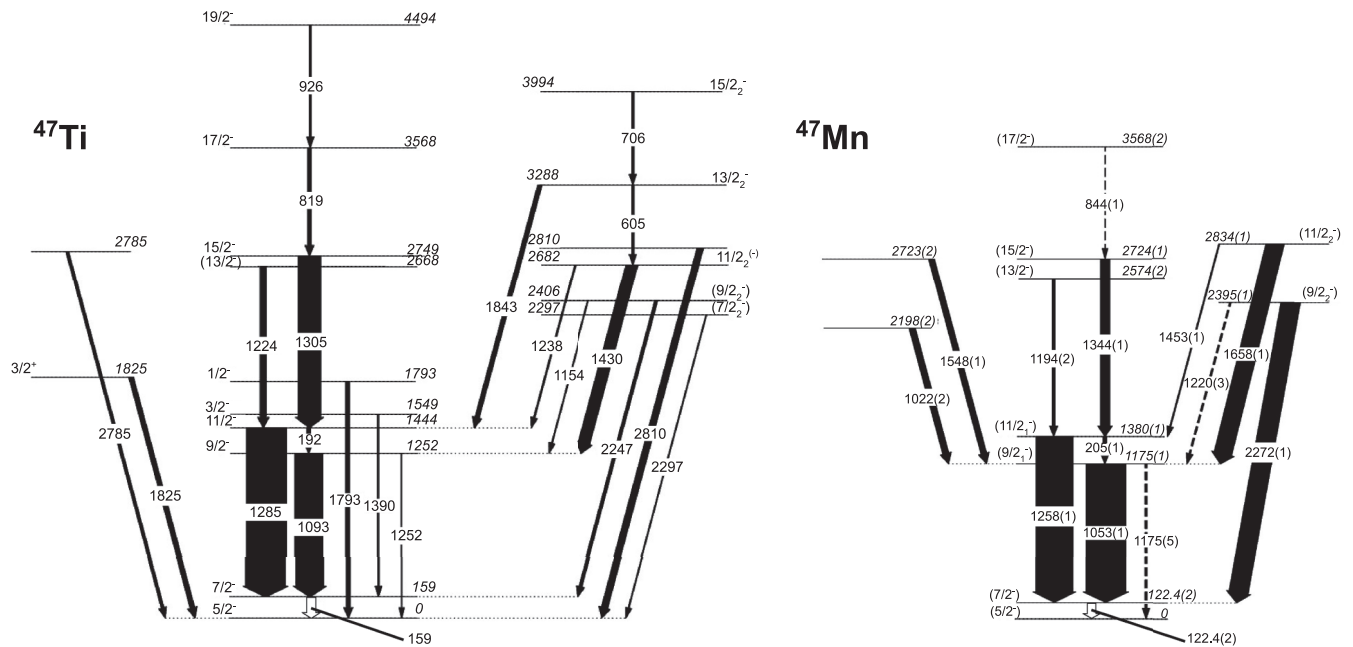
FIG. 3. The partial level scheme for ^{47}Ti as observed in this work and the new ^{47}Mn level scheme. The J^π values for ^{47}Mn are tentatively assigned since they are based on mirror symmetry arguments. States of some transitions observed in ^{47}Mn have not been assigned a J^π value as the corresponding mirror transitions were not seen in ^{47}Ti. Energies quoted for ^{47}Ti are taken from previous measurements [21]. The widths of the solid arrows are proportional to the efficiency-corrected intensities. The relative intensities of the decays from the first-excited states (hollow arrows) have not been measured. All γ-ray intensities are presented relative to that obtained for the 1285-keV transition in ^{47}Ti and the 1053-keV transition in ^{47}Mn. Tentative placement of transitions is indicated using dashed lines.

populated directly via one-nucleon knockout from the $f_{7/2,5/2}$ and $p_{3/2,1/2}$ orbitals from the 4^+ ground state of the ^{48}V secondary beam. The $\frac{1}{2}^-$ and $\frac{15}{2}^-$ states can only be populated through removal of an $f_{7/2}$ proton, while the other states may involve the high-lying fp orbitals. Although $J^\pi = \frac{15}{2}^-$ is the maximum spin that can be populated directly by an fp-shell knockout, states of higher spin, beyond $\frac{15}{2}^-$, were observed to be weakly populated. This suggests the possibility of these states being populated either through unobserved γ-ray feeding from higher-lying lower-J states which have been directly populated, from an unobserved, weakly populated, high-J isomeric state in the beam, or by some higher-order reaction mechanism.

The 2668-keV state in ^{47}Ti, from which the 1224-keV transition is observed to decay, is listed in the literature [21] as $J = \frac{9}{2}$ or $\frac{13}{2}$. The observation in the current knockout experiment suggests negative parity, in which case this state would be either the yrast $\frac{13}{2}_1^-$ state or the $\frac{9}{2}_3^-$ state. The current evaluation [21] suggested that while $J = \frac{13}{2}$ would be preferred, its lack of observation in some fusion-evaporation reactions may point to a more likely assignment of $J = \frac{9}{2}$. However, we note that Cameron *et al.* observed a 1223-keV γ-ray transition, which we assume to be the same one, using a heavy-ion fusion-evaporation reaction [26], even though this transition was not ultimately placed in their scheme. We suggest that it is unlikely for a $\frac{9}{2}_3^-$ state to be populated in preference to

the yrast $\frac{13}{2}_1^-$ state in a fusion reaction, and so we tentatively assign this state as the $J^\pi = \frac{13}{2}_1^-$ state.

Only one positive-parity state, with $J^\pi = \frac{3}{2}^+$, was observed in ^{47}Ti which can only be populated directly through knockout from the $d_{5/2}$ orbital. Furthermore, current evaluation data for ^{47}Ti [21] can only assign a range of possible J^π values for the states at 2785 and 2810 keV, which are also observed in this work.

Figure 2(d) shows the newly observed γ rays emitted from the excited states of the proton-rich nucleus, ^{47}Mn. The errors in the γ-ray energies come both from the statistical error of the fit and the systematic errors associated with the uncertainties in the recoil residue velocity and the target position. All γ rays labeled in Fig. 2(d) have been placed in a new level scheme—see the right side of Fig. 3. The strongest transitions were initially placed in the scheme using mirror-symmetry arguments, and the placement of the γ-ray transitions in the scheme has been confirmed though a γ-γ coincidence analysis and using intensity arguments. Example coincidence spectra, gated on the 1194- and 1658-keV transitions, are shown in Figs. 2(e) and 2(f) respectively. These are the equivalent spectra for the analog transitions of 1224 and 1430 keV; see Figs. 2(b) and 2(c). The same coincidence pattern is clearly seen for the mirror partners.

The 122-keV transition labeled in Fig. 2(d) is clearly the analog of the 159-keV transition in ^{47}Ti and a similarly long low-energy tail is observed—again indicating that, as with the

analog transition, the decaying state has a long lifetime of the order of hundreds of ps. To determine the precise γ-ray energy an analysis identical to that in Ref. [15] has been performed in which the experimental spectrum was fitted with a simulation to extract, simultaneously, the energy of the transition and the lifetime of the state. The full analysis and a discussion of the lifetime will be published in a forthcoming paper. For the purpose of the current work, only the γ-ray energy is needed, and the value of 122.4(2) keV was obtained using the procedure as outlined in Ref. [15].

Spin and parity assignments for the newly observed states are made on the basis of mirror symmetry arguments— through comparison of the state energies, γ-ray energies, decay patterns, and population intensities. Because these are "mirrored" direct reactions, isospin symmetry suggests that similar distributions of direct population strength should be observed, and this assumption is also used to inform the spin-parity assignments.

The correspondence between the analog states of the two main yrast sequences ($J^{\pi} = \frac{5}{2}^{-}, \frac{7}{2}^{-}, \frac{9}{2}^{-}, \frac{11}{2}^{-}, \frac{13}{2}^{-}$, and $\frac{15}{2}^{-}$) is reasonably clear, due to the observed interleaving transitions and energy similarities. A γ-γ coincidence analysis suggests that an 844-keV transition feeds the 2724-keV state, and the resulting 3568-keV state is tentatively assigned as the yrast $\frac{17}{2}^{-}$ state. As in ^{47}Ti, this state cannot be directly populated in the reaction and must be populated indirectly or from an isomer.

The tentative assignment of the 2834-keV state as $\frac{11}{2}^{-}_{2}$ is made following the observation that, in ^{47}Ti, the strongest transition feeding the yrast $\frac{9}{2}^{-}$ state is from the nonyrast $\frac{11}{2}^{-}_{2}$ state, which seems to be strongly populated in this knockout reaction. Assuming a similarly strong population of the analog $\frac{11}{2}^{-}_{2}$ state in the mirrored reaction, a strong transition feeding the 1175-keV state in ^{47}Mn would be expected. The 1548- or 1658-keV transitions, which are observed to feed the 1175-keV state, are the only reasonable candidates for the analog of the 1430-keV transition. Since the 1658-keV line is by far the strongest, we tentatively assign the 2834-keV state as the $\frac{11}{2}^{-}_{2}$ state. We note that this state also decays to the yrast $\frac{11}{2}^{-}_{1}$ state—a pattern seen for the analog 2682-keV state in ^{47}Ti.

Similarly, for the 2395-keV state, we observe that this decays by a strong high-energy transition (2272 keV) to the first excited state. Comparison with the decay patterns in ^{47}Ti show that the nonyrast $\frac{9}{2}^{-}_{2}$ gains direct population and feeds the first excited state with a transition of similar energy (2247 keV). We therefore tentatively assign the 2395-keV state in ^{47}Mn as $\frac{9}{2}^{-}_{2}$. In addition, a weak 1220-keV transition is observed that may correspond to a decay from this state to the $\frac{9}{2}^{-}_{1}$ state, in which case this would be the analog of the 1154-keV transition in ^{47}Ti. This 1220-keV transition is too weak for a γ-γ analysis and hence this placement is tentative. Two other states are observed in ^{47}Mn at 2198 and 2723 keV. We have not been able to identify analog states in ^{47}Ti to which these might correspond.

A summary of the states observed to be populated in this work, the measured γ-ray energies and the relative intensities of the transitions in ^{47}Ti and ^{47}Mn is given in Table II.

Intensities (and hence cross sections; see Sec. III D) were measured using the spectra without the add-back procedure applied and were obtained with Gaussian fits. For the low-energy decays from the two long-lived analog first-excited states, accurate intensity measurements could not be made due to lack of reliable information on the absolute γ-ray efficiency. This is due to the fact that the line shape covers a wide range of energies, extending to well below 100 keV in both cases, where efficiency is not well determined. In addition, for the lifetimes concerned, one half-life corresponds to decay positions several cm downstream of the target, and decays >10 cm downstream of the target will contribute to the photo peak, resulting in a significant uncertainty in geometrical efficiency.

The level schemes of Fig. 3 indicate that, of the excited states, the knockout process seems to preferentially populate the first excited state, $J^{\pi} = \frac{7}{2}^{-}$, the yrast and yrare states with $J^{\pi} = \frac{9}{2}^{-}$ and $\frac{11}{2}^{-}$ and the $J^{\pi} = \frac{15}{2}^{-}$ state, with the two yrare states populated roughly as strongly as their corresponding yrast states.

Later, in Sec. III D, we make a detailed comparison of experimental and theoretical cross sections for the observed states. However, it is useful at this point to make a qualitative comparison of these experimental observations with the predicted distribution of one-nucleon knockout strength across all the low-lying states accessible through knockout. For this purpose, we have calculated theoretical knockout cross sections, for the lowest three states of each J^{π} between $\frac{1}{2}^{-}$ and $\frac{15}{2}^{-}$. These predictions use a combination of eikonal reaction dynamics assuming a spectator-core approximation (e.g., Refs. [27,28]), Hartree-Fock-constrained nucleon form factors, and shell-model spectroscopic factors. The latter were obtained in the full fp space using the KB3G [29] interaction using the ANTOINE code [30,31]. Further details can be found in Sec. III D. Figure 4 shows the results for ^{47}Mn. Only states that carry a theoretical cross section of $\geqslant 0.1\%$ of the total cross section are presented. As experimentally observed, the first and second $J^{\pi} = \frac{9}{2}^{-}$ and $\frac{11}{2}^{-}$ states are predicted to be very strongly populated, along with the ground state and first excited state. Thus, there is broad agreement between the experimental and theoretical distributions of knockout strength. It is also interesting to note that while Fig. 3 indicates that the $\frac{15}{2}^{-}$ state in ^{47}Mn is populated with significant intensity, the calculated cross section for this state is negligible. Experimentally, it is possible that, like the $J^{\pi} = \frac{17}{2}^{-}$ state, there is unseen feeding from other high-spin states into the $J^{\pi} = \frac{15}{2}^{-}$ state.

B. ^{45}Cr level scheme

The Doppler-corrected γ-ray spectra for the ^{45}Sc/^{45}Cr mirror nuclei are presented in Fig. 5 and were obtained following the same procedure as for the $A = 47$ mirror pair described above.

The γ-ray spectrum in coincidence with the ^{45}Sc outgoing nucleus is shown in Fig. 5(a). These γ rays were observed following two-proton removal from ^{47}V. Again it is important to note that this reaction is expected to be a combination of direct ($2p$ knockout) and indirect reactions (proton knockout

TABLE II. The measured experimental exclusive cross sections (in mb) for the states observed in the $A = 47$ mirror pair in this work. The measured level energies (E_{J_i}) and γ-ray energies in ^{47}Mn are presented with errors (in keV). The level energies and γ-ray energies in ^{47}Ti are quoted in accordance to the energies measured in Refs. [21]. The measured level energies presented have been applied to determine the theoretical cross sections of each state. The relative intensities (R.I.) of the decays observed for both nuclei are presented. The experimental and theoretical exclusive cross sections are presented for both nuclei, as well as the experimental inclusive cross sections. The theoretical inclusive cross section for ^{47}Ti has not been computed due to the restricted shell-model space utilized; see Sec. III D for details.

	^{47}Ti		^{47}Mn			^{47}Ti				^{47}Mn			
$J_i^{\pi(a)}$	σ_{exp} (mb)	σ_{th} (mb)	σ_{exp} (mb)	σ_{th} (mb)	$J_i^\pi \to J_f^{\pi(a)}$	E_γ	E_i	E_f	R.I.	E_γ	E_i	E_f	R.I.
$\frac{5}{2}^-_{\mathrm{gs}}$	–[b]	2.95	–[c]	2.44	–	0	0	0	–	0	0	0	–
$\frac{7}{2}^-_1$	–[b]	2.07	–[c]	1.77	$\frac{7}{2}^-_1 \to \frac{5}{2}^-_{\mathrm{gs}}$	159	159	0	–[d]	122.4(2)	122.4(2)	0	–[d]
$\frac{9}{2}^-_1$	5.5(8)	4.16	0.4(2)	3.34	$\frac{9}{2}^-_1 \to \frac{7}{2}^-_1$	1093	1252	159	70(3)	1053(1)	1175(1)	122.4(2)	100(5)
					$\frac{9}{2}^-_1 \to \frac{5}{2}^-_{\mathrm{gs}}$	1252	1252	0	0.9(6)	1175(5)	1175(1)	0	5(4)
$\frac{11}{2}^-_1$	4(2)	6.15	1.4(2)	4.93	$\frac{11}{2}^-_1 \to \frac{7}{2}^-_1$	1285	1444	159	100(5)	1258(1)	1380(1)	122.4(2)	93(5)
					$\frac{11}{2}^-_1 \to \frac{9}{2}^-_1$	192	1444	1252	9.8(9)	205(1)	1380(1)	1175(1)	10(2)
$\frac{3}{2}^-_1$	0.8(5)	0.07	–	–	$\frac{3}{2}^-_1 \to \frac{7}{2}^-_1$	1390	1549	159	4(3)	–	–	–	–
$\frac{1}{2}^-_1$	1.9(7)	0.03	–	–	$\frac{1}{2}^-_1 \to \frac{5}{2}^-_{\mathrm{gs}}$	1793	1793	0	10(3)	–	–	–	–
$\frac{3}{2}^+_1$	2(1)	–	–	–	$\frac{3}{2}^+_1 \to \frac{5}{2}^-_{\mathrm{gs}}$	1825	1825	0	12(5)	–	–	–	–
$(\frac{7}{2}^-_2)$	0.4(4)	0.95	–	–	$(\frac{7}{2}^-_2) \to \frac{5}{2}^-_{\mathrm{gs}}$	2297	2297	0	2(2)	–	–	–	–
$(\frac{9}{2}^-_2)$	1.8(8)	4.75	1.1(1)	4.26	$(\frac{9}{2}^-_2) \to \frac{7}{2}^-_1$	2247	2406	159	7(4)	2272(1)	2395(1)	122.4(2)	49(5)
					$\frac{9}{2}^-_2 \to \frac{9}{2}^-_1$	1154	2406	1252	2(1)	1220(3)	2395(1)	1175(1)	4(3)
$(\frac{13}{2}^-_1)$	2.9(8)	1.61	0.15(9)	1.34	$(\frac{13}{2}^-_1) \to \frac{11}{2}^-_1$	1224	2668	1444	15(4)	1194(2)	2574(2)	1380(1)	7(4)
$\frac{11}{2}^{(-)}_2$	5.1(8)	5.00	1.0(1)	4.35	$\frac{11}{2}^{(-)}_2 \to \frac{9}{2}^-_1$	1430	2682	1252	29(2)	1658(1)	2834(1)	1175(1)	45(4)
					$\frac{11}{2}^{(-)}_2 \to \frac{11}{2}^-_1$	1238	2682	1444	3(3)	1453(1)	2834(1)	1380(1)	3(1)
$\frac{15}{2}^-_1$	9(1)	0.00	0.45(8)	0.00	$\frac{15}{2}^-_1 \to \frac{11}{2}^-_1$	1305	2749	1444	57(5)	1344(1)	2724(1)	1380(1)	24(4)
$\frac{13}{2}^-_2$	2(1)	0.59	–	–	$\frac{13}{2}^-_2 \to \frac{11}{2}^-_1$	1843	3288	1444	11(4)	–	–	–	–
					$\frac{13}{2}^-_2 \to \frac{11}{2}^{(-)}_2$	605	3288	2682	5(1)	–	–	–	–
$\frac{17}{2}^-_1$	0.8(4)	–	0.03(2)	–	$\frac{17}{2}^-_1 \to \frac{15}{2}^-_1$	819	3568	2749	9(1)	844(1)	3568(2)	2724(1)	1(1)
$\frac{15}{2}^-_2$	1.0(7)	0.00	–	–	$\frac{15}{2}^-_2 \to \frac{13}{2}^-_2$	706	3994	3288	5(4)	–	–	–	–
$\frac{19}{2}^-_1$	0.9(3)	–	–	–	$\frac{19}{2}^-_1 \to \frac{17}{2}^-_1$	926	4494	3568	5(1)	–	–	–	–
-	–	–	0.3(2)	–	$- \to \frac{9}{2}^-_1$	–	–	–	–	1022(2)	2198(2)	1175(1)	16(9)
-	–	–	0.29(6)	–	$- \to \frac{9}{2}^-_1$	–	–	–	–	1548(1)	2723(2)	1175(1)	15(3)
-	1.32(98)	–	–	–	$- \to \frac{5}{2}^-_{\mathrm{gs}}$	2785	2785	0	7(5)	–	–	–	–
-	3(1)	–	–	–	$- \to \frac{5}{2}^-_{\mathrm{gs}}$	2810	2810	0	16(5)	–	–	–	–
inclusive	96(6)	–	8.1(5)	22.4									

[a]The J^π assignments listed are those for ^{47}Ti.
[b]The combined cross section for the ground state and the $\frac{7}{2}^-_1$ state for ^{47}Ti is 53(7) mb; see text for details.
[c]The combined cross section for the ground state and the $\frac{7}{2}^-_1$ state for ^{47}Mn is 3.0(6) mb; see text for details.
[d]The efficiency-corrected absolute intensity (hence relative intensity) could not be determined for this transition; see text for details.

followed by proton evaporation) and hence, unlike the $A = 47$ mirrors above, this reaction cannot be considered the analog of the reaction used to produce ^{45}Cr. In order to determine the optimum velocity for the Doppler correction, the 1237-keV transition ($\frac{11}{2}^- \to \frac{7}{2}^-_{\mathrm{gs}}$) in ^{45}Sc was utilized since the adopted lifetime of the decaying state of 2.6(1) ps [33] indicates that the γ ray is emitted from within the target. The resulting optimum velocity $\beta = 0.383(5)$ was used in Figs. 5(a)–5(c). The transitions labeled in Fig. 5(a) are all well known from previous work [12,34,35]. The $J^\pi = \frac{3}{2}^+$ 12-keV state has a lifetime of 326 ms, and hence its decay is not observable. The cascade of γ rays observed in ^{45}Sc in this work is presented

in the partial level scheme on the left panel in Fig. 6. In this reaction, both the negative- and positive-parity structures are observed. The latter structure forms a regular rotational band built on the low-lying $J^\pi = \frac{3}{2}^+$ state, presumably formed from a $d_{3/2}$ proton excitation, driving the nucleus to a deformed shape [32]. Some example γ-γ coincidence spectra, gated on the 543- and 962-keV transitions, are shown in Figs. 5(b) and 5(c). All energies and coincidence relations measured in this work were found to be consistent with those reported in Refs. [12,32,33].

Through two-proton knockout from the fp-shell, negative-parity states up to a maximum of $J^\pi = \frac{15}{2}^-$ are populated,
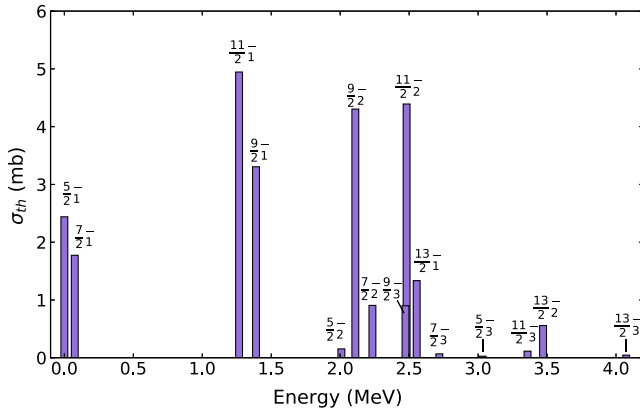
FIG. 4. The predicted cross sections (see text for details) for the lowest three predicted states of each J^π between $\frac{1}{2}^-$ and $\frac{15}{2}^-$ in ^{47}Mn. The excitation energy shown is from the shell-model calculations. States that have theoretical cross sections below 0.1% of the total predicted cross section are not shown—this applies to all three states of $J^\pi = \frac{15}{2}^-$.

resulting from direct two-proton removal from the $J^\pi = \frac{3}{2}^-$ ground state of the ^{47}V secondary beam. Similarly, a maximum of $J^\pi = \frac{15}{2}^+$ may be populated (e.g., by removal of one $f_{7/2}$ and one $d_{5/2}$ proton). Figure 6 shows that states up to, and beyond, both these limits are weakly observed. This indicates that, as with the $A = 47$ case, indirect processes (which will be present since in this case $-2p$ knockout is not a direct process) may be important in the population of these higher-spin states, or weakly populated high-J isomers may be present in the secondary beam.

The only state tentatively known in ^{45}Cr is the location of the $J^\pi = \frac{3}{2}^+$ isomer [36]. A long-lived (>80 μs) isomer, decaying by a 107(1)-keV γ-ray transition, was observed in ^{45}Cr in a decay-spectroscopy experiment following a fragmentation reaction. This was assumed to be the analog of the 12-keV $J^\pi = \frac{3}{2}^+$ state in ^{45}Sc—the only isomeric state known in that nucleus. This information was crucial in establishing the new level scheme of ^{45}Cr as described below.

Figure 5(d) shows the γ-ray spectrum for the $T_z = -\frac{3}{2}$ ^{45}Cr residues produced via the two-neutron knockout reaction from the $T_z = -\frac{1}{2}$ ^{47}Cr beam. For the Doppler correction, the optimum velocity of 0.386(5) was obtained using the 1245(2)-keV transition. Guided by mirror-symmetry arguments and using a γ-γ coincidence analysis and γ-ray intensities, as described below, all the transitions labeled in Fig. 5(d) have been tentatively placed in a new level scheme for ^{45}Cr shown in the right panel in Fig. 6.

Of the labeled transitions in Fig. 5(d), three pairs of γ rays are separated by 107(1) keV—the energy of the $J^\pi = \frac{3}{2}^+$ isomer in ^{45}Cr (the 947/1054-, 516/622-, and 385/492-keV transitions)—and hence, given their high intensity, these are assumed to decay from three separate low-lying states, all three of which decay to both the $J^\pi = \frac{3}{2}^+$ isomer and the $J^\pi = \frac{7}{2}^-$ ground state. Through comparison with the level scheme in Fig. 6 (left), the analog pairs of transitions in ^{45}Sc are

most likely the 962/974-, 531/543-, and 364/377-keV transitions, respectively. Hence, the decaying states in ^{45}Cr were tentatively assigned as $J^\pi = \frac{7}{2}^+$, $\frac{5}{2}^+$, and $\frac{3}{2}_1^-$, respectively. Despite very low statistics, a γ-γ coincidence analysis was successfully deployed to help tentatively place the remaining transitions, as outlined below.

The broad grouping of transitions around 1060 keV in Fig. 5(d) was found to be in self-coincidence, pointing to the existence of two transitions around this energy forming a cascade; see Fig. 5(f). Indeed, close inspection of this peak reveals that it is too wide for a single transition, and a double-Gaussian fit with a fixed peak width reveals two transitions of 1054(2) and 1065(2) keV; see Fig. 7(a). A third Gaussian was included in the fit which reveals a weak 1090(2)-keV transition. Figure 7(b) shows the result of gating on the left (around 1054 keV) and the right (around 1065 keV) of this transition. Both show the coincidence relationship, and a slight separation of the γ-ray energies is noticeable in Fig. 7(b), as would be expected. The order of these two transitions cannot be made on the basis of intensity, but the 107-keV difference between the 947- and 1054-keV transitions suggests that the 1054-keV transition is the lower one. Therefore, the resulting 2119-keV state is tentatively assigned as the $J^\pi = \frac{11}{2}^+$ state, through comparison with the ^{45}Sc scheme. Statistics were not sufficient to confirm the placement of the 947-keV transition, and so the placement here remains tentative, based only on the 107-keV energy difference compared with the 1054-keV transition. We speculate that the 1090(2)-keV transition may be from the $J^\pi = \frac{13}{2}^+$ state, based on mirror symmetry arguments. A coincidence analysis adds no information, due to low statistics, and therefore, the placement of this transition was not added in the level scheme in Fig. 6.

If the tentative assignment of the new 622-keV $J^\pi = \frac{5}{2}^+$ state is correct, then mirror symmetry arguments might suggest that the 898-keV transition feeds into it—the analog of the 891-keV transition in ^{45}Sc. However, this is ruled out by intensity arguments and there is no hint of this in the coincidence data. Instead, a gate on the 622-keV transition suggests, despite very low statistics, a coincidence with a transition at 881(2) keV, see Fig. 5(e). The 881-keV transition appears as a tail on the 898-keV transition in Fig. 5(d). This points to a state at 1503 keV, which we tentatively assign as the $J^\pi = \frac{9}{2}^+$ state. Statistics were not sufficient to confirm the placement of the 516-keV transition, and again its placement remains tentative, based only on the 107-keV energy difference compared with the 622-keV transition. The low statistics for this sequence of states means that their placement must be considered tentative.

Both the 385- and 492-keV transitions are clearly observed to be in coincidence with the 566-keV transition, yielding a state at 1058 keV. Comparison with the ^{45}Sc scheme reveals only one possible analog—the $J^\pi = \frac{3}{2}_2^-$ state.

The remaining two unplaced strong transitions, the 898- and 1245-keV transitions, have been analyzed in the γ-γ analysis. These transitions are not observed to be in mutual coincidence and the 898-keV transition has a higher intensity than the 1237-keV transition. This rules out the possibility that the 898-keV transition is the analog of the 870-keV
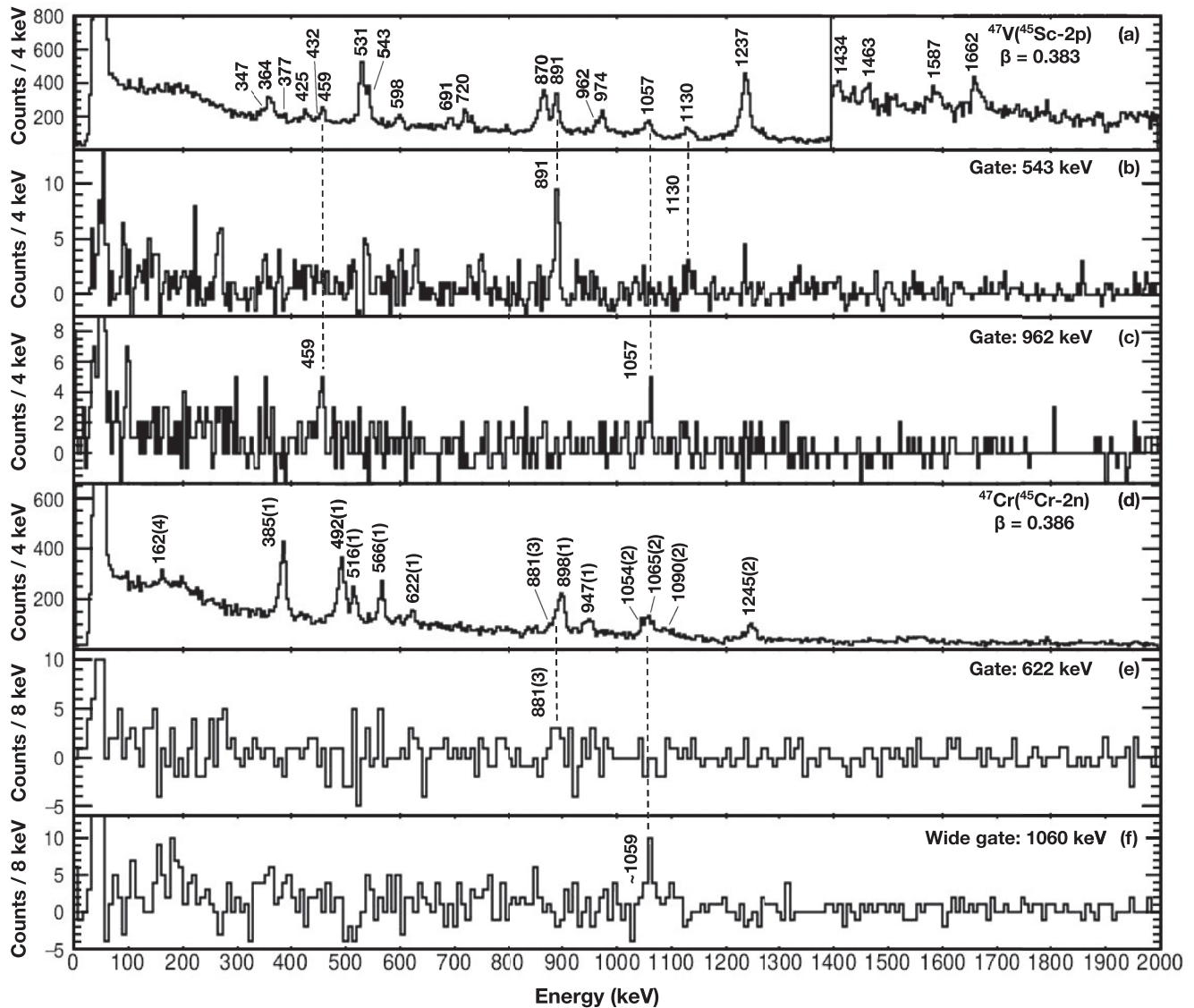
FIG. 5. The Doppler-corrected spectra, using add-back (see text), for (a) ^{45}Sc and (d) ^{45}Cr from two-nucleon removal reactions from ^{47}V and ^{47}Cr, respectively. The β value utilized for both (a) and (d) was optimized for "fast" transitions: 1237 keV in ^{45}Sc and its analog transition of 1245 keV in ^{45}Cr. Panels (b) and (c) show γ-γ coincidence spectra by gating on the 543- and 962-keV transitions in ^{45}Sc. The respective γ-γ coincidence analysis for their analog transitions in ^{45}Cr are shown in (e) and (f) by gating on the 622- and 1060-keV transitions, respectively, the latter being a broad gate covering both the 1054- and 1065-keV transitions (see text).

$J^{\pi} = \frac{15}{2}^{-} \rightarrow \frac{11}{2}^{-}$ transition. Indeed, neither of these transitions exhibit any strong coincidences. Hence they are likely to be directly populated and feed into either the ground state or the isomer. The 1245-keV transition is assigned as the analog of the 1237-keV $J^{\pi} = \frac{11}{2}^{-} \rightarrow \frac{7}{2}^{-}_{gs}$ transition, which is very strongly populated in ^{45}Sc. There is no evidence for a $J^{\pi} = \frac{15}{2}^{-} \rightarrow \frac{11}{2}^{-}$ transition. Comparing with the ^{45}Sc scheme, the candidate for the analog to the 898-keV transition is the 720-keV $J^{\pi} = \frac{5}{2}^{-} \rightarrow \frac{7}{2}^{-}_{gs}$ transition. If the resulting 898-keV state were the analog of the $J^{\pi} = \frac{5}{2}^{-}$ state in ^{45}Sc, then it may, as with ^{45}Sc, be fed by a low-energy transition from the $J^{\pi} = \frac{3}{2}^{-}_{2}$ state; in this case the transition would be 162 keV. A weak 162-keV transition is indeed observed in Fig. 5(d) and is

therefore placed in the scheme. A summary of the states identified in this work in the $A = 45$ mirror nuclei, the measured γ-ray energies and the relative intensities of the transitions is given in Table III.

Although the placement of the transitions in the new ^{45}Cr scheme and the resulting J^{π} assignments should be considered tentative, being based in part on mirror symmetry arguments, it is challenging to find any other reasonable arrangement of the observed γ rays. Moreover, all the observed ^{45}Cr transitions have been placed in the new scheme and all the states observed below 1.5 MeV in ^{45}Sc have an analog state identified in ^{45}Cr. It can be seen from Fig. 6 that the population intensity of the low-lying negative-parity states, $J^{\pi} = \frac{3}{2}^{-}_{1}$, $\frac{3}{2}^{-}_{2}$, and $\frac{5}{2}^{-}$, is significantly larger, in relative terms, in ^{45}Cr
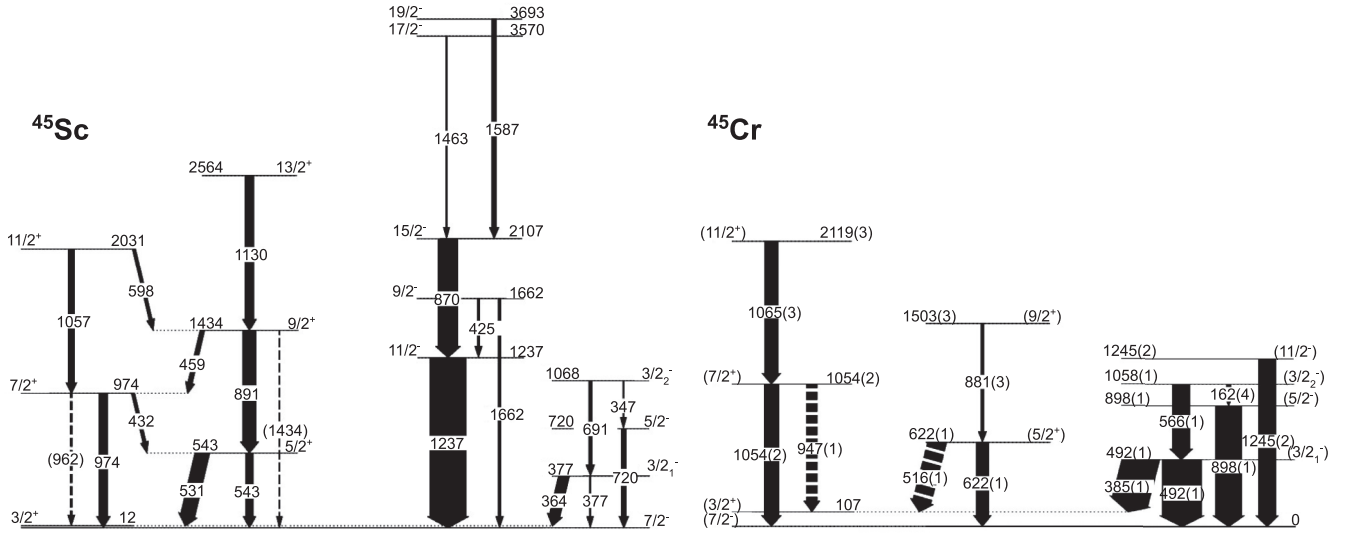
FIG. 6. The level schemes observed in this work for ^{45}Sc and ^{45}Cr. The spins and parities of ^{45}Cr are tentative, being based on mirror-symmetry arguments. Tentative placement of transitions is indicated using dashed lines. Energies labeled for ^{45}Sc are taken from more precise previous measurements [12,32]. The widths of the arrows are proportional to the relative efficiency-corrected γ-ray intensities (see text). All γ-ray intensities are presented relative to the $\frac{3}{2}^-$ to $\frac{7}{2}^-$ transition in ^{45}Cr and to the $\frac{11}{2}^-$ to $\frac{7}{2}^-$ transition in ^{45}Sc.

compared to that of their analog states in ^{45}Sc. It is also notable that these states are not populated at all in fusion-evaporation reactions such as Ref. [12]. This suggests that these states may have direct population in both reactions–i.e., from the *direct* $-2n(-2p)$ channel to ^{45}Cr (^{45}Sc). If this is the case, then the relative population intensity between these three states would be expected to be similar in each member of the mirror pair, since the two-nucleon amplitudes (which reflect the spectroscopic overlap for the direct reaction) would be expected to be identical due to isospin symmetry. Using
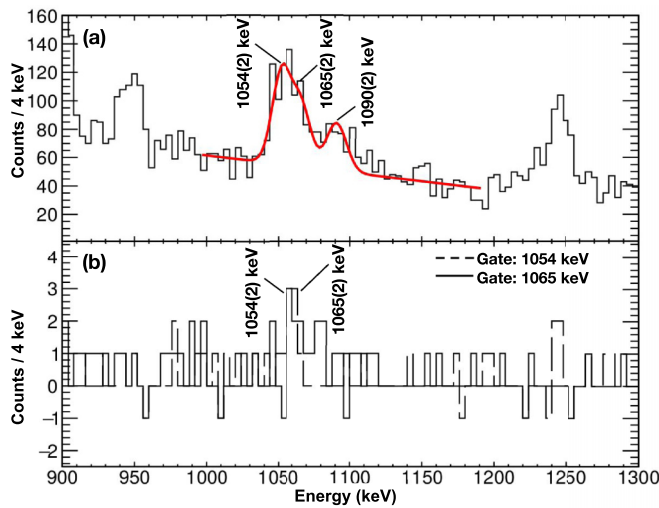

FIG. 7. The Doppler-corrected spectra of ^{45}Cr where (a) shows the fitting procedure of the 1054(2)- and 1065(2)-keV peaks. The corresponding γ-γ coincidences for the 1054(2)- and 1065(2)-keV peaks are shown in (b) where the dashed (solid) spectrum corresponds to the that measured in coincidence with 1054(1065)-keV peak, respectively.

the relative intensities of the transitions feeding into and out of these three states, it is possible to determine the relative population of these states. For the ^{47}Cr $-2n \rightarrow ^{45}$Cr reaction, the population intensity for the $J^\pi = \frac{3}{2}^-_1, \frac{3}{2}^-_2$, and $\frac{5}{2}^-$ are in the ratio 100(9):37(6):37(6) while for the ^{47}V $-2p \rightarrow ^{45}$Sc reaction they are in the ratio 100(21):52(14):42(21). These ratios are the same, within errors, which gives further confidence to the assignments made in ^{45}Cr.

Finally, as with the case of the $A = 47$ mirror nuclei above, it is instructive to make a theoretical prediction of the distribution of knockout strength among the low-lying states of ^{45}Cr, to compare with the experiment. For this purpose, we have calculated theoretical two-neutron knockout cross sections for the ^{47}Cr $-2n \rightarrow ^{45}$Cr reaction. The two-neutron removal cross sections were calculated following the prescription in Refs. [28,37], combining shell-model structure input with eikonal reaction dynamics and the assumption that the two nucleons are removed suddenly from the projectile. The residual nucleus is assumed to act as a spectator during the reaction. Two-nucleon amplitudes (TNA) were calculated with the KB3G interaction [29] in the full fp space, using the NuShellX@MSU code [38]. The TNA contain the nuclear structure input and represent the amplitudes for each two-nucleon configuration with J^π, coupled to final residue state J^π_f, in the projectile ground state J^π_i. As in the single-nucleon removal calculations, the valence nucleon radial wave functions were calculated in a Woods-Saxon plus spin-orbit potential, the geometry of which was constrained by Hartree-Fock calculations.

The shell-model space used for the knockout cross-section calculations restricts the calculations to negative-parity final states only. The results are shown in Fig. 8, which presents the predicted cross section for all accessible states that are calculated to occur below the ^{45}Cr proton separation

TABLE III. The measured level energies (E_{J_i}) and γ-ray energies for the $A = 45$ mirror nuclei (in keV). The level energies and γ-ray energies in ^{45}Sc are taken from Ref. [12]. The relative intensities (R.I.) of the decays observed are presented relative to the 1237-keV transition in ^{45}Sc and to the 492-keV transition in ^{45}Cr.

$J^\pi_i \to J^{\pi\,(a)}_f$	^{45}Sc				^{45}Cr			
	E_γ	E_{J_i}	E_{J_f}	R.I.	E_γ	E_{J_i}	E_{J_f}	R.I.
$\frac{3}{2}^-_1 \to \frac{7}{2}^-_{gs}$	377	377	0	4(2)	492(1)	492(1)	0	100(8)
$\frac{3}{2}^-_1 \to \frac{3}{2}^+_1$	364	377	13	29(4)	385(1)	492(1)	107(1)	97(8)
$\frac{5}{2}^+_1 \to \frac{7}{2}^-_{gs}$	543	543	0	20(4)	622(1)	622(1)	0	32(10)
$\frac{5}{2}^+_1 \to \frac{3}{2}^+_1$	531	543	13	40(4)	516(1)	622(1)	107(1)	47(7)
$\frac{5}{2}^-_1 \to \frac{7}{2}^-_{gs}$	720	720	0	13(5)	898(1)	898(1)	0	67(6)
$\frac{7}{2}^+_1 \to \frac{7}{2}^-_{gs}$	974	974	0	24(4)	1054(2)	1054(2)	0	40(9)
$\frac{7}{2}^+_1 \to \frac{3}{2}^+_1$	962	974	13	6(2)	947(1)	1054(2)	107(1)	27(8)
$\frac{7}{2}^+_1 \to \frac{5}{2}^+_1$	432	974	543	8(5)	–	–	–	–
$\frac{3}{2}^-_2 \to \frac{3}{2}^-_1$	691	1068	377	9(3)	566(1)	1058(1)	492(1)	45(7)
$\frac{3}{2}^-_2 \to \frac{5}{2}^-_1$	347	1068	720	3(2)	162(4)	1058(1)	898(1)	11(6)
$\frac{11}{2}^-_1 \to \frac{7}{2}^-_{gs}$	1237	1237	0	100(6)	1245(2)	1245(2)	0	44(7)
$\frac{9}{2}^+_1 \to \frac{5}{2}^+_1$	891	1434	543	36(4)	881(3)	1503(3)	622(1)	7(3)
$\frac{9}{2}^+_1 \to \frac{7}{2}^+_1$	459	1434	974	12(3)	–	–	–	–
$\frac{9}{2}^+_1 \to \frac{7}{2}^-_{gs}$	1434	1434	0	3(1)	–	–	–	–
$\frac{9}{2}^-_1 \to \frac{7}{2}^-_{gs}$	1662	1662	0	7(2)	–	–	–	–
$\frac{9}{2}^-_1 \to \frac{11}{2}^-_1$	425	1662	1237	6(3)	–	–	–	–
$\frac{11}{2}^+_1 \to \frac{7}{2}^+_1$	1057	2031	974	17(5)	1065(3)	2119(3)	1054(2)	41(9)
$\frac{11}{2}^+_1 \to \frac{9}{2}^+_1$	598	2031	1434	9(2)	–	–	–	–
$\frac{15}{2}^-_1 \to \frac{11}{2}^-_1$	870	2107	1237	55(4)	–	–	–	–
$\frac{13}{2}^+_1 \to \frac{9}{2}^+_1$	1130	2564	1434	23(5)	–	–	–	–
$\frac{17}{2}^-_1 \to \frac{15}{2}^-_1$	1463	3570	2107	4(2)	–	–	–	–
$\frac{19}{2}^-_1 \to \frac{15}{2}^-_1$	1587	3693	2107	13(4)	–	–	–	–

^{a}The J^π assignments listed are those for ^{45}Sc.

energy of 3.0 MeV. These cross sections are plotted as a function of the shell-model excitation energy. Even though this shell-model space does not reproduce well the excitation en-
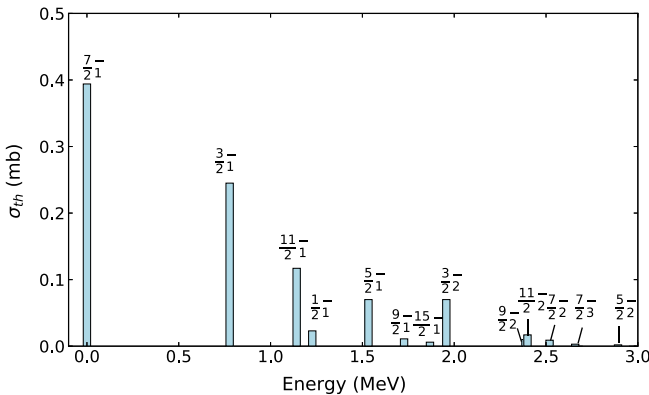

FIG. 8. Theoretical cross sections for all states predicted to lie below the proton separation energy (≈ 3 MeV) in ^{45}Cr. Shell-model energies were used in the reaction model to determine the two-neutron knockout theoretical cross sections. See text for details.

ergies of some of the states, the key features of the predictions are in broad agreement with what is observed. First, the four negative-parity excited states that are observed experimentally to be populated directly in ^{45}Cr, the $J^\pi = \frac{3}{2}^-_1$, $\frac{3}{2}^-_2$, $\frac{5}{2}^-$, and $\frac{11}{2}^-$ states have the largest predicted cross sections. Second, the $J^\pi = \frac{15}{2}^-$ state has a very small predicted cross section, consistent with the nonobservation of this state for ^{45}Cr.

C. Mirror energy differences

Having determined the level schemes for ^{47}Mn and ^{45}Cr, the experimental MED for the ^{47}Ti/^{47}Mn and ^{45}Sc/^{45}Cr mirror nuclei can be established for the states observed. In the following sections, the experimental MED are discussed and compared with the results of two theoretical approaches—a large-scale shell-model method and a recently developed approach based on DFT.

The large-scale shell-model calculations for the ^{47}Mn/^{47}Ti and ^{45}Sc/^{45}Cr pairs were performed using ANTOINE [30,31]. The KB3G interaction [29] was used in the full fp-valence space, without any truncation within that space. The

approach, for the negative-parity states, follows exactly that of Refs. [2,11]. In this method, four isospin-breaking components were included, with each contributing separately to the MED calculation. The four terms are as follows:

(a) *Coulomb multipole term* (usually referred to as V_{CM}): This term accounts for the multipole Coulomb interaction between protons and is included by the addition of Coulomb matrix elements to the effective two-body interaction of protons.

(b) *Additional isovector term* (V_B): It has been found, in the fp shell in particular, that the Coulomb multipole term is, on its own, unable to account for all the multipole contributions to the MED. It was found [10,11] that, across the entire region, an additional effective isovector term needed to be included systematically to account for the experimental data. The contribution of this term to the MED is of the same order as the Coulomb multipole term (many tens of keV). It was shown [2] that this effect has a strong J dependence and that, for the most part, it is the $J = 0$ component that dominates. On the basis of this, in this work, the additional isovector term V_B is included only for $J = 0$ couplings of protons and is set to -100 keV (i.e., 100 keV more attractive for all fp protons than for neutrons).

(c) *Single-particle shifts* (V_{ll} and V_{ls}): This accounts for the Coulomb, and electromagnetic spin-orbit [39,40] single-particle shifts. These are included following the prescription of Ref. [10].

(d) *Radial term* (V_{Cr}): This is a monopole term that takes into account the changes in the nuclear radius as a function of the angular momentum. This is determined from the mean occupation of the $p_{\frac{3}{2}}$ orbitals and follows the prescription of Ref. [11]. The application of these methods to $T_z = \pm\frac{3}{2}$ nuclei in the fp shell builds on the earlier work of Refs. [5,6,41] for the $A = 49$, 51, and 53 $T_z = \pm\frac{3}{2}$ mirror pairs.

Regarding the shell-model description of the positive-parity final states observed in $f_{7/2}$-shell nuclei, there is no available interaction that allows for both sd-shell and fp-shell particles to be considered fully in the same valence space. However, in the ^{45}Sc/^{45}Cr mirror pair, a low-lying deformed positive-parity structure is observed to exist very close to the ground state. The $J^\pi = \frac{3}{2}^+$ bandhead is generally considered to be based principally on a single particle-hole excitation from the $d_{3/2}$ orbit. Indeed, the $[202]\frac{3}{2}$ Nilsson level, originating from $d_{3/2}$, reaches the Fermi level for $N, Z = 21$ for a well-deformed prolate shape. Hence, to examine the MED for these positive-parity structures, a shell-model calculation is presented which uses the SDPF interaction [42], which includes the sd-shell orbitals in addition to the fp orbitals and which allows for one particle-hole excitation from the $d_{\frac{3}{2}}$ orbital (proton excitation for ^{45}Sc and a neutron excitation in ^{45}Cr). The calculation, and the various multipole and monopole contributions to the MED, was otherwise performed exactly as for the negative-parity states. MED results from this approach are presented for the $A = 45$ case.

A recent, alternative theoretical study from Bączyk and Satuła [14] has led to the development of a new approach to determining MED through multireference DFT [13]. The NCCI method [14] was employed, which allows for the complete treatment of rotational and isospin symmetries. Isospin-breaking effects originating from Coulomb and nuclear (CSB) interactions are included, where next-to-leading order (NLO) contact terms were implemented for the latter interaction [43], the parameters for which were obtained from global fits to displacement energies [13]. This method, being based on a mean-field theory with fitted global parameters, represents a very different approach from the shell model. The method was first applied by Llewellyn *et al.* [15] to the heaviest-studied mirror pair, the $T_z = \pm\frac{1}{2}$ $A = 79$ mirrors—a region where the required shell-model space make practical calculations intractable. It is interesting to compare the two methods in this work. The DFT method is described in more detail in Ref. [13], in which a bench-marking of the new approach, compared with the shell-model results, is also presented. Further details of the specific DFT-NCCI method, and the configurations used, can be found in the Supplemental Material [44]. Results from both the shell-model and DFT approaches are presented in the following sections.

1. MED results for ^{47}Ti/^{47}Mn

The calculated and experimental MED for the observed states in ^{47}Ti/^{47}Mn are compared in Fig. 9. All MED plotted are normalized to the $\frac{5}{2}^-$ ground state. The data in Fig. 9(a) (open circles) show a negative MED, reducing to roughly -75 keV before increasing back toward zero. Variations in MED of about 100 keV are typical of Coulomb multipole effects associated with the recoupling of pairs of protons from $J = 0$ to J_{max} in one of the members of the mirror pair (see, e.g., Ref. [11]). A change in trend in the MED (e.g., negative trend followed by positive trend, as in this case) may indicate that both types of nucleon are recoupling both members of the mirrors.

The blue line in Fig. 9(a) presents the MED obtained from the shell-model calculation, which includes all four isospin-breaking effects described in Sec. III C. A systematic shift of ≈ 30–40 keV is seen between the calculated results and experiment for the yrast states. Since MED are normalized to the ground state, this might indicate a poor description of the $J^\pi = \frac{5}{2}^-$ ground states. The $J^\pi = \frac{13}{2}^-$ state is plotted in parentheses due to the tentative assignment of this state in ^{47}Ti. The agreement for this state is poor. For the observed yrare states [see insert in Fig. 9(a)], the $\frac{11}{2}_2^-$ state is not well reproduced by the calculations; however, a better agreement was seen for the $\frac{9}{2}_2^-$ state. Some aspects of the poor agreement with the shell model are likely to be due to the inadequacy of the fp space for this mirror pair. Indeed, only two protons (neutrons) are present in ^{47}Ti (^{47}Mn) in this valence space. It is possible that missing two-particle two-hole excitations across the ^{40}Ca shell closure will contribute to this discrepancy. This mirror pair will provide a useful test to any model that incorporates both the lower fp shell and the upper sd shell.

The MED for the yrast states using the DFT-NCCI method are represented by the triangles in Fig. 9(a)—again normal-
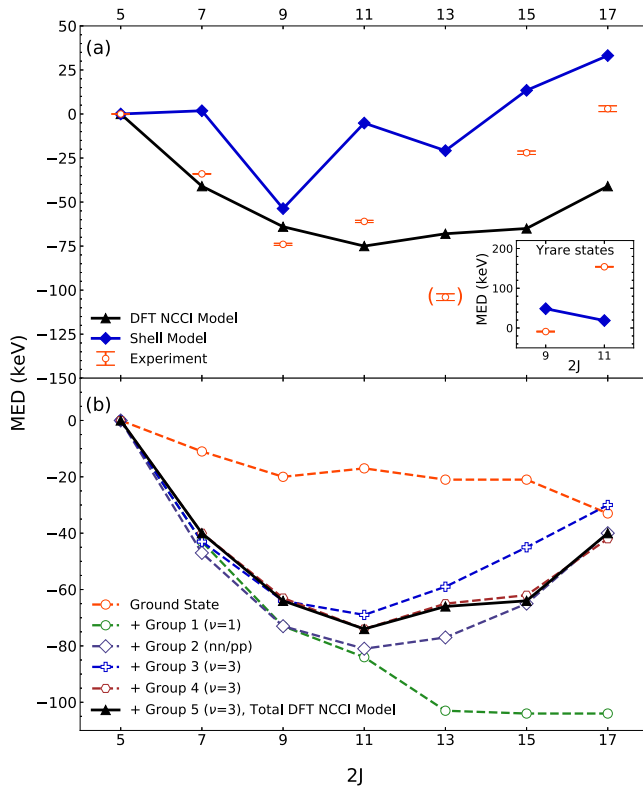
FIG. 9. (a) Mirror energy differences as a function of spin $2J$ for the ^{47}Mn/^{47}Ti mirror pair. The solid blue line (diamonds) represents the shell-model MED which includes all four isospin-breaking interactions (see text). The black line (triangles) represents the MED calculated from the DFT-NCCI approach. The red points refer to the experimental MED. The $\frac{13}{2}^-_1$ state is presented in parenthesis due to its tentative assignment. The inset in (a) shows the MED as a function of spin J for the observed yrare analog states in the ^{47}Mn/^{47}Ti pair. (b) The DFT-NCCI calculations shown as a function of $2J$ demonstrating how the various configuration types contribute to the final result, denoted by the black triangles in (a). See text for details.

ized to the $\frac{5}{2}^-$ ground state. This calculation is based on 23 Hartree-Fock configurations, the inclusion of which was found to be sufficient to converge the calculations as discussed in Fig. 9(b). The different lines in Fig. 9(b) show the contributions of different types of excited configuration. The plot shows the cumulative effect of adding, sequentially, five different excited-configuration types on top of the ground-state configuration, the MED for which are shown by red circles/dashed line. The sequence, in which the configurations were added, is as follows:

(i) (Group 1): seniority $\nu = 1$ configurations (open green circles), in which there are no fully broken pairs, and hence reflect the possible different locations of the odd unpaired particle;

(ii) (Group 2) (open diamonds): states built on like-particle (nn, pp) pair excitations;

(iii) (Group 3) (open crosses): $\nu = 3$ configurations based on the lowest-energy broken-pair excitations;

(iv) (Group 4) (open hexagons): same as Group 3 but for broken pairs in the odd subsystem;

(v) (Group 5) (triangles): additional seniority $\nu = 3$ configurations which represent other low lying even and odd subsystem broken-pair excitations.

This final line contains all configuration types and is therefore equivalent to the black line (triangles) in Fig. 9(a). See Supplemental Material [44] for more details on the specific configurations used.

It is interesting to note that the inclusion of the ground-state configuration plus Groups 1 and 2 above ($\nu = 1$ and pair excitations) produces an MED [see diamonds in Fig. 9(b)] that has the correct trend; i.e., an initially negative trend followed by a positive trend. Thus the overall trend can be reproduced through particle angular-momentum alignments but without fully breaking pairs. The inclusion of the $\nu = 3$ configurations on top does not significantly change the outcome, overall. The overall agreement from the full DFT calculation [black line (triangles) in Fig. 9(a)] is good at lower spins and matches the trend well overall, although the numerical agreement is poorer for the higher-spin states.

2. MED results for ^{45}Sc/^{45}Cr

The experimental MED for the $A = 45$ mirror nuclei are shown in Fig. 10(a) for the negative-parity states and Fig. 10(b) for the positive-parity states; see open circles. For the negative-parity states the MED are plotted relative to the $J^\pi = \frac{7}{2}^-$ ground state, while the positive-parity MED are plotted relative to the $J^\pi = \frac{3}{2}^+$ bandhead state.

The blue line/diamonds in Fig. 10(a) show that the shell model provides a good description of the $\frac{11}{2}^-_1$ state and the $\frac{3}{2}^-_2$ state (see insert) but fails badly for the $\frac{3}{2}^-_1$ and $\frac{5}{2}^-_1$ states. Again, the inadequacy of the fp space may be an issue here since the fp model space only has one proton (neutron) present in ^{45}Sc (^{45}Cr). For example, if the $\frac{3}{2}^-_1$ and $\frac{5}{2}^-_1$ states involve excitations of this single particle to the $p_{3/2}$ and $f_{5/2}$ levels, then this state may not be well described in this shell-model space. The purple line/squares in Fig. 10(b) show, for the positive-parity states, the theoretical MED for the SDPF-shell-model calculation based on the excitation of a single $d_{3/2}$ nucleon in ^{45}Sc/^{45}Cr. The agreement with the experiment MED is very good. Both the theoretical and experimental MED are relatively small in magnitude without large variation from state to state, indicating that a stable deformed configuration persists along this rotational sequence.

In the DFT approach the configuration space does not need to be truncated, and configurations based on sd-shell and pf-shell excitations can be included on an equal footing and are required for the positive-parity states. The DFT-NCCI results are shown in Fig. 10(a) for the negative-parity states and Fig. 10(b) for the positive-parity states. Again, further details on the configurations used can be found in the Supplemental Material [44].

It can be seen that the agreement with the data is poor in both sequences of states. This is the first case (see Ref. [13]) where the DFT-NCCI fails to reproduce the overall sign and trend of the MED. We cannot currently account for this
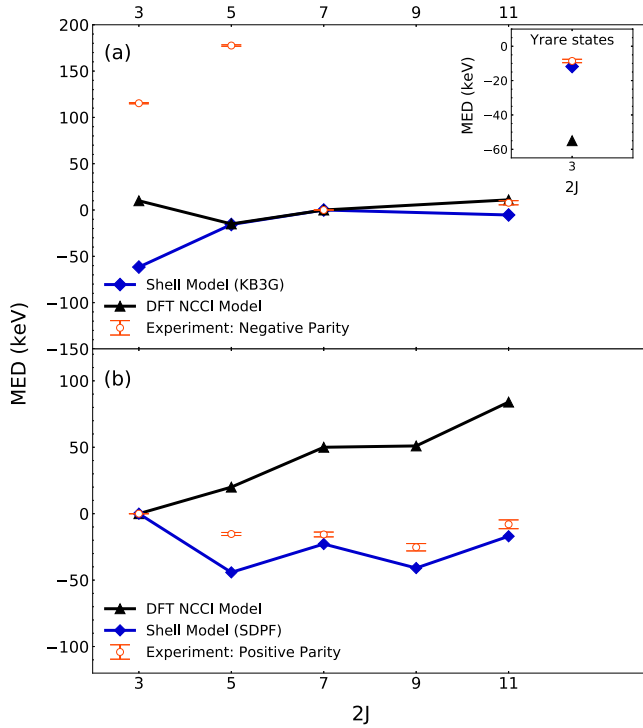
FIG. 10. (a) MED as a function of spin $2J$ for the ^{45}Sc/^{45}Cr nuclei for the negative-parity states. The blue line (diamonds) represents the shell-model MED calculations that include the four isospin-breaking interactions (see text). The black line (triangles) represents the DFT-NCCI approach and the red open circles refer to the experimental MED. The inset in (a) shows the MED as a function of spin J for the observed analog yrare $\frac{3}{2}\frac{-}{2}$ states. (b) The MED as a function of spin J for the observed positive-parity states. The DFT-NCCI approach used for the ^{45}Sc/^{45}Cr mirror pair, denoted by the black line (triangles). The blue line (diamonds) represents the MED from the SDPF shell-model calculation, and the experimental MED are represented by the red open circles.

FIG. 11. A test calculation of MED (see text) as a function of spin $2J$ for the positive-parity states in the ^{45}Sc/^{45}Cr nuclei. The calculation has been performed using three different variants of isospin-breaking force including: the Coulomb force (blue squares), the Coulomb plus nuclear LO CSB (green diamonds) of Ref. [45], and the Coulomb plus nuclear NLO CSB (red dots) of Ref. [43]. In the test calculation 11 low-lying configurations were included.

11 low-lying configurations. The result is shown in Fig. 11. This confirms the relatively strong sensitivity of the MED to the form of CSB force. Data of the kind presented here may therefore present an opportunity to fine-tune the low-energy coupling constants of the NLO CSB force. However, it should be noted that, in all three cases, the calculated MED is positive—at variance with experimental data and the result of the shell-model calculation.

D. Knockout cross sections in the $A = 47$ mirror pair

Experimental one-nucleon knockout cross sections have been measured for populating ^{47}Ti and ^{47}Mn. Both inclusive σ_{inc} (summed over all observed states) and exclusive σ_{excl} (for individual states) have been determined. Inclusive cross sections were determined from incoming and outgoing particle intensities, following efficiency and dead-time corrections, for each reaction, with normalization achieved through comparison of data from reaction and transmission settings of the S800. Exclusive cross sections were then determined, for each observed state, using the efficiency-corrected γ-ray intensities and γ-ray feeding from higher energy states into the state of interest. The experimentally determined exclusive and inclusive cross sections for both nuclei are presented in Table II. As described in Sec. III A, it was not possible to measure the intensity for the decays from the two $\frac{7}{2}\frac{-}{1}$ first-excited states. Hence exclusive cross sections could not be determined. Instead, we determine a combined cross section for the ground state and the $\frac{7}{2}\frac{-}{1}$ from the difference between the inclusive cross section and the sum of all the measured exclusive cross sections of the remaining excited states. This yields 3.0(6) mb for ^{47}Mn and 53(7) mb for ^{47}Ti. These combined cross sections are used for comparisons with theoretical cross sections later in this section.

The theoretical one-nucleon knockout cross sections for each of the observed individual states in $A = 47$ mirror nuclei were calculated using eikonal reaction dynamics by

discrepancy, but it could be indicative of missing correlations in the model, especially for the negative-parity states where the calculated spectrum is in rather poor agreement with the experimental data. For positive-parity states the energy-spectrum agreement is better, but the calculated band appears, from the energy spacing, to be too collective when compared to data. Another reason could be related to the nuclear NLO CSB interaction. Its (three) coupling constants were adjusted globally to the binding energies or, precisely, to the mirror displacement energies. Such a fit establishes an overall magnitude of the CSB force which is sufficient for mean-field applications but is completely insensitive to its matrix elements which enter the DFT-NCCI theory through configuration mixing. In order to test how sensitive the calculated MED are, to the form of the charge-symmetry-breaking force, we performed test calculations for the positive-parity states in ^{45}Sc/^{45}Cr nuclei using three different variants of the model that include (1) the Coulomb interaction, (2) the Coulomb plus leading order (LO) CSB forces [45], and (3) the Coulomb plus NLO CSB forces [43]. In the test calculation we included only
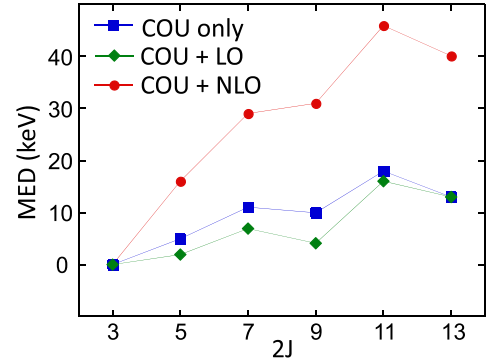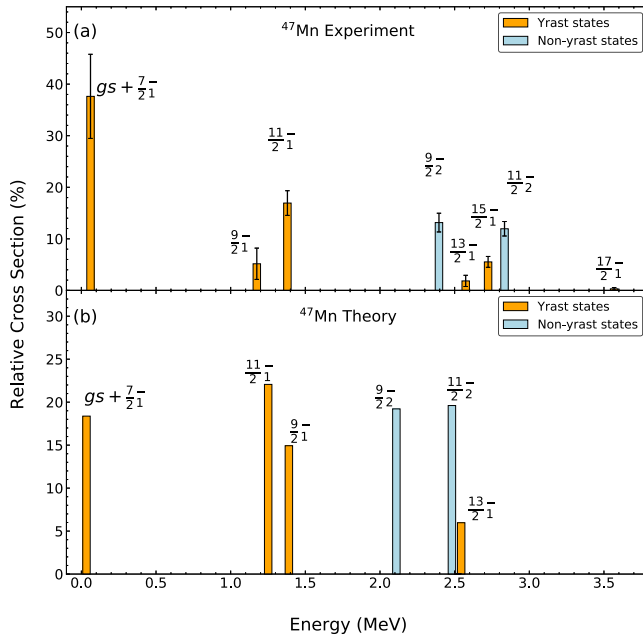
FIG. 12. (a) Experimental and (b) calculated relative cross section for the observed excited states in ^{47}Mn as a result of the one-neutron knockout from the 4^+ ground state of ^{48}Mn. The theoretical relative cross section for the populated $\frac{15}{2}^-$ state was found to be close to zero and is excluded from the figure.

assuming a spectator-core approximation (e.g., Refs. [27,28]). Valence-nucleon radial wave functions were calculated in a Woods-Saxon plus spin-orbit potential, the geometry of which was constrained by Hartree-Fock calculations [18]. Spectroscopic factors were obtained from the shell model using the ANTOINE code [30,31], with calculations performed in the full fp model space using the KB3G interaction [29]. The calculated exclusive cross sections for both nuclei are presented in Table II. In relation to inclusive cross sections, it is customary [20] to calculate the theoretical inclusive cross section as the sum of the individual cross sections for all bound final states, which is 4.2 mb in this case. This value includes only the ground state and first excited state, since the proton separation energy is $S_p = 384$ keV [46] in ^{47}Mn. Since we see direct population of states well above this energy, we instead define the theoretical inclusive cross section here as the sum of the calculated cross sections of all observed states. The mirror nucleus ^{47}Ti is, in contrast, a strongly bound system, with proton and neutron separation energies of $S_p = 10.46$ MeV and $S_n = 8.88$ MeV, respectively [46]. Its theoretical inclusive cross section was not determined since the calculation of all bound states in the shell model would involve an unfeasibly large number of states.

Considering the proton-rich member of the mirror pair, ^{47}Mn, Figs. 12(a) and 12(b) show the comparison of the relative experimental and theoretical cross sections as a function of experimental excitation energy for ^{47}Mn. The relative cross section is defined as $\sigma_{\text{excl}}/\sigma_{\text{inc}}$. In both Figs. 12(a) and 12(b), the cross sections for the $\frac{5}{2}^-$ ground state and the $\frac{7}{2}^-_1$ first-excited state are combined, and the average excita-

tion energy is used in both cases. Generally, the comparison shows that the experimental and theoretical relative cross sections share some key features, specifically that the cross sections to excited states are dominated by the five states with $J^\pi = \frac{5}{2}^-_1$, $\frac{9}{2}^-_{1,2}$, and $\frac{11}{2}^-_{1,2}$. The strong direct population of the nonyrast states with $J^\pi = \frac{9}{2}^-_2$ and $\frac{11}{2}^-_2$ states is also well reproduced. It is worth noting that the $J^\pi = \frac{15}{2}^-_1$ state receives strong population in the data, but the calculated direct population cross section is negligibly small. This again implies that high-spin states may be subject to some other indirect population process.

The inclusive cross section for the one-neutron knockout of ^{48}Mn to ^{47}Mn was measured to be $8.10 \pm 0.05\text{(stat.)} \pm 0.48\text{(sys.)}$ mb, with the final error dominated by fluctuations of the purity of the incoming beam. The theoretical inclusive cross section was found to be 22.4 mb for ^{47}Mn, a factor of ≈ 3 larger. Since sd-shell removal to bound states is possible, as indicted by the population of the $J^\pi = \frac{3}{2}^+$ state in ^{47}Ti, and that this possibility is excluded from our model space, the theoretical cross section is certainly underestimated. The suppression of experimental cross sections for knockout reactions on light targets, compared to the theoretical cross sections of the kind presented here, is a feature in recent studies [18–20]. In those works, the suppression is observed to be dependent on the (a)symmetry of the separation energies between the two nucleon species. Specifically, a correlation was observed with ΔS, defined as $S_n - S_p$ for neutron knockout and $S_p - S_n$ for proton knockout. Relevant to the current work, the systematics show that removal of strongly bound neutrons from a weakly bound system along the proton-drip line may be expected to show suppression of the cross section compared with theory. In the present work, for the purpose of the inclusive cross section, ΔS was determined to be 14.4 MeV for ^{47}Mn using the method described in Ref. [20] for cases where multiple states have been populated. For this value of ΔS, the systematics presented in Ref. [20] suggests $R_s = \sigma_{\text{exp}}/\sigma_{\text{th}}$ to be 0.38(10) which compares well the value in this work of 0.36(2).

Turning to the results of the mirrored reaction, ^{48}V to ^{47}Ti via a proton knockout, as summarized in Table II, a number of observations can be made. First, the measured inclusive cross section of $96.2 \pm 0.3\text{(stat.)} \pm 5.6\text{(sys.)}$ is a factor of ≈ 11 higher than the equivalent measurement made in its mirror nucleus. Second, for many of the strongly populated yrast states in ^{47}Ti, the individual exclusive cross sections are much larger than the theoretical values—which is not the case for the mirrored reactions to the analog states in ^{47}Mn. These observations are consistent with those of Yajzey et $al.$ [8]. That study, which also performed mirrored knockout reactions, in that case one neutron (proton) removal from ^{49}Fe (^{49}V) to ^{48}Fe (^{48}Ti) observed similar patterns in the comparison of the mirrored reactions. The analysis presented in Ref. [8] was undertaken with data taken in the same experiment as the current work.

Yajzey et $al.$ [8] interpreted the above observations in terms of binding energy effects, in which the large binding energy of the positive T_z member of the pair for both protons and neutrons, compared with the low proton separation energy of the negative T_z member, results in the observed asymmetric

behavior. Specifically, it was proposed in Ref. [8] that essentially all fp- and sd-shell removal paths will most likely populate bound states in the positive T_z nucleus, yielding a large inclusive cross section. Conversely, in the proton-rich mirror nucleus, the excitation energy centroids of the single-particle strength distribution for sd-shell removal will be significantly above the proton separation energy and hence will decay by proton emission, resulting in a lower inclusive cross section corresponding almost entirely to fp-shell removal. In the current work, where $S_p = 10.46$ MeV and $S_n = 8.88$ MeV for ^{47}Ti, and $S_p = 0.38$ MeV and $S_n = 18.22$ MeV for ^{47}Mn [46], the conditions for similar behavior are present.

As in Ref. [8], in this interpretation, there is likely to be significant unseen feeding into the yrast states of ^{47}Ti, inflating the measured exclusive cross sections. Indeed, the very large combined cross section of 53(7) mb for the ground state and first excited state suggests that there must be significant unseen feeding into these states. Yajzey *et al.* made an estimate of the maximum (sum-rule) cross section, based on the assumption of full sd shells and three protons in the fp shell (for $Z = 23$ ^{49}V), and that knockout from all these subshells populates bound states in ^{48}Ti. This estimate was 139 mb. Since the current work corresponds to proton-knockout from the neighboring isotope, ^{48}V, under the same experimental conditions, then the same estimate is valid here, too.

As an exercise, we can take this maximum fp- plus sd-shell removal cross section as the theoretical inclusive cross section, yielding a lower limit of R_s of 0.69(4) for proton knockout from ^{48}V to ^{47}Ti. Using the calculated ΔS of 1.8 MeV for this case, this again compares favorably with the systematics presented in Ref. [20] which suggests R_s to be 0.58(10).

Taken together with the results of Ref. [8], the current work suggests that binding-energy effects are crucial in understanding the patterns of behavior in mirrored knockout reactions, a technique that has now been employed a number of times; e.g., Refs. [5,8,16,17]. In addition, this also indicates that the comparison of experimental *exclusive* cross cross sections in analog (mirrored) reactions may be compromised by the effects of unseen feeding in the strongly bound member of the mirror pair.

IV. CONCLUSIONS

New states and corresponding γ-ray transitions have been identified in the proton-rich ^{47}Mn and ^{45}Cr ($T_z = -\frac{3}{2}$) nuclei.

This represents the first in-beam γ-ray spectroscopic study of either nucleus, resulting in new level schemes for both nuclei. This has been achieved by utilizing the mirrored-knockout approach, coupled to a γ-γ coincidence analysis, with spins and parities assigned through mirror symmetry arguments. Mirror energy differences have been investigated for the ^{47}Ti/^{47}Mn and ^{45}Sc/^{45}Cr mirror pairs for the first time, including comparison of the data with results from the established shell-model approach and from a new DFT method. The agreement with the data generally is reasonable for the shell-model approach, though with poor agreement for some specific states, presumably explained by the small number of particles in the model space. The comparison of data with the DFT has mixed success, reasonable for $A = 47$ and poor for $A = 45$. Areas for future investigation have been presented. A discussion of the mirrored knockout (one-nucleon) cross sections for the $A = 47$ mirror pair is presented, including a successful comparison of experimental and theoretical exclusive cross sections for one-neutron removal to ^{47}Mn. The large asymmetry in the inclusive cross sections between the $A = 47$ mirror pair was discussed in terms of binding-energy effects.

The processed experimental data generated during the current study are available in the University of York repository [47].

[1] E. Wigner, Phys. Rev. **51**, 106 (1937).

[2] M. A. Bentley, S. M. Lenzi, S. A. Simpson, and C. A. Diget, Phys. Rev. C **92**, 024310 (2015).

[3] M. A. Bentley *et al.*, Phys. Rev. Lett. **97**, 132501 (2006).

[4] J. Ekman *et al.*, Phys. Rev. Lett. **92**, 132502 (2004).

[5] S. A. Milne *et al.*, Phys. Rev. C **93**, 024318 (2016).

[6] P. J. Davies *et al.*, Phys. Rev. Lett. **111**, 072501 (2013).

[7] K. Kaneko, Y. Sun, T. Mizusaki, and S. Tazaki, Phys. Rev. Lett. **110**, 172505 (2013).

[8] R. Yajzey *et al.*, Phys. Lett. B **823**, 136757 (2021).

[9] A. Fernández *et al.*, Phys. Lett. B **823**, 136784 (2021).

[10] A. P. Zuker, S. M. Lenzi, G. Martínez-Pinedo, and A. Poves, Phys. Rev. Lett. **89**, 142502 (2002).

[11] M. A. Bentley and S. M. Lenzi, Prog. Part. Nucl. Phys. **59**, 497 (2007).

[12] P. Bednarczyk *et al.*, Eur. Phys. J. A **2**, 157 (1998).

[13] P. Bączyk and W. Satula, Phys. Rev. C **103**, 054320 (2021).

[14] W. Satuła, P. Bączyk, J. Dobaczewski, and M. Konieczka, Phys. Rev. C **94**, 024306 (2016).

[15] R. Llewellyn *et al.*, Phys. Lett. B **811**, 135873 (2020).

[16] K. Wimmer *et al.*, Phys. Lett. B **785**, 441 (2018).

[17] M. Spieker *et al.*, Phys. Rev. C **99**, 051304(R) (2019).

[18] A. Gade *et al.*, Phys. Rev. C **77**, 044306 (2008).

[19] J. A. Tostevin and A. Gade, Phys. Rev. C **90**, 057602 (2014).

[20] J. A. Tostevin and A. Gade, Phys. Rev. C **103**, 054610 (2021).

[21] T. Burrows, Nucl. Data Sheets **108**, 923 (2007).

[22] D. Morrissey, B. Sherrill, M. Steiner, A. Stolz, and I. Wiedenhoever, Nucl. Instrum. Methods B **204**, 90 (2003).

[23] D. Bazin, J. Caggiano, B. Sherrill, J. Yurkon, and A. Zeller, Nucl. Instrum. Methods B **204**, 629 (2003).

[24] D. Weisshaar *et al.*, Nucl. Instrum. Methods B **847**, 187 (2017).

[25] S. Paschalis *et al.*, Nucl. Instrum. Methods B **709**, 44 (2013).

[26] J. Cameron *et al.*, Phys. Lett. B **235**, 239 (1990).

[27] P. Hansen and J. Tostevin, Annu. Rev. Nucl. Part. Sci. **53**, 219 (2003).

[28] E. C. Simpson, J. A. Tostevin, D. Bazin, B. A. Brown, and A. Gade, Phys. Rev. Lett. **102**, 132502 (2009).

[29] A. Poves, J. Sánchez-Solano, E. Caurier, and F. Nowacki, Nucl. Phys. A **694**, 157 (2001).

[30] E. Caurier and F. Nowacki, Acta Phys. Pol. B **30**, 705 (1999).

[31] E. Caurier, G. Martinez-Pinedo, F. Nowack, A. Poves, and A. P. Zuker, Rev. Mod. Phys. **77**, 427 (2005).

[32] P. Bednarczyk *et al.*, Acta Phys. Pol. B **32**, 747 (2001).

[33] T. Burrows, Nucl. Data Sheets **109**, 171 (2008).

[34] D. C. Tayal, K. P. Singh, and H. S. Hans, Phys. Rev. C **34**, 1262 (1986).

[35] M. Matejska-Minda *et al.*, Acta Phys. Pol. B **51**, 829 (2020).

[36] R. Hoischen *et al.*, J. Phys. G: Nucl. Part. Phys. **38**, 035104 (2011).

[37] J. A. Tostevin and B. A. Brown, Phys. Rev. C **74**, 064604 (2006).

[38] B. A. Brown and W. D. M. Rae, Nucl. Data Sheets **120**, 115 (2014).

[39] D. R. Inglis, Phys. Rev. **82**, 181 (1951).

[40] J. Nolen, Jr. and J. Schiffer, Annu. Rev. Nucl. Sci. **19**, 471 (1969).

[41] J. R. Brown *et al.*, Phys. Rev. C **80**, 011306(R) (2009).

[42] A. Poves and J. S. Solano, Phys. Rev. C **58**, 179 (1998).

[43] P. Bączyk, W. Satuła, J. Dobaczewski, and M. Konieczka, J. Phys. G: Nucl. Part. Phys. **46**, 03LT01 (2019).

[44] See Supplemental Material at http://link.aps.org/supplemental/10.1103/PhysRevC.106.024327 which includes Refs. [48–53], for details of the NCCI calculations, the procedure followed and the configurations used.

[45] P. Bączyk, J. Dobaczewski, M. Konieczka, W. Satuła, T. Nakatsukasa, and K. Sato, Phys. Lett. B **778**, 178 (2018).

[46] M. Wang, W. Huang, F. Kondev, G. Audi, and S. Naimi, Chin. Phys. C **45**, 030003 (2021).

[47] University of York Research Database: 10.15124/539e7a2a-8077-4045-ad56-9e26f9b46a12.

[48] J. Dobaczewski, W. Satuła, B. Carlsson, J. Engel, P. Olbratowski, P. Powałowski, M. Sadziak, J. Sarich, N. Schunck, A. Staszczak, M. Stoitsov, M. Zalewski, and H. Zduńczuk, Comput. Phys. Commun. **180**, 2361 (2009).

[49] J. Dobaczewski, P. Bączyk, P. Becker, M. Bender, K. Bennaceur, J. Bonnard, Y. Gao, A. Idini, M. Konieczka, M. Korteleinen, L. Próchniak, A. Romero, W. Satuła, Y. Shi, T. Werner, and L. Yu, J. Phys. G: Nucl. Part. Phys. **48**, 102001 (2021).

[50] N. Schunck, J. Dobaczewski, W. Satuła, P. Bączyk, J. Dudek, Y. Gao, M. Konieczka, K. Sato, Y. Shi, X. Wang, and T. Werner, Comput. Phys. Commun. **216**, 145 (2017).

[51] W. Satuła, J. Dobaczewski, W. Nazarewicz, and M. Rafalski, Phys. Rev. Lett. **103**, 012502 (2009).

[52] M. Beiner, H. Flocard, N. V. Giai, and P. Quentin, Nucl. Phys. A **238**, 29 (1975).

[53] W. Satuła and J. Dobaczewski, Phys. Rev. C **90**, 054303 (2014).